KeAi

CHINESE ROOTS
GLOBAL IMPACT

Contents lists available at ScienceDirect

Petroleum Science

journal homepage: www.keaipublishing.com/en/journals/petroleum-science



Original Paper

Pressure transient behavior of fractured wells in multilayered tight gas reservoirs with heterogeneous properties and limited fracture height



Jing-Jing Guo *, Chao-Zhi Jiang, Hai-Tao Wang **, Lie-Hui Zhang

State Key Laboratory of Oil and Gas Reservoir Geology and Exploitation, Southwest Petroleum University, Chengdu, 610500, Sichuan, China

ARTICLE INFO

Article history: Received 16 September 2024 Received in revised form 8 May 2025 Accepted 8 May 2025 Available online 8 May 2025

Edited by Yan-Hua Sun

Keywords: Multi-layer gas reservoir Commingled production Pressure transient analysis Limited fracture height Interlayer interference

ABSTRACT

Hydraulic fracturing and commingle production of multiple layers are extensively adopted in unconventional tight gas reservoirs, Accurate determination of parameters of individual layers in multilayered tight gas reservoirs is essential for well performance evaluation and development strategy optimization. However, most analytical models for fractured vertical wells in stratified gas reservoirs focus on fully penetrated hydraulic fractures, neglecting the influence of partial penetration of hydraulic fractures. This paper presents a semi-analytical model to investigate the transient pressure behavior of vertically fractured wells in dual porosity multi-layered tight gas reservoirs. The partial penetration of hydraulic fracture, the vertical heterogeneities of layer properties, the differences between hydraulic fracture lengths in each layer and the stress sensitivity are all incorporated in the proposed model. The pointsource solution, Laplace transformation, Fourier transformation, Pedrosa's transformation, perturbation technique, and the superposition principle are applied to obtain the analytical solution of transient pressure responses. The proposed model is validated against a commercial software, and the transient pressure behavior of vertically fractured wells in multi-layered tight gas reservoirs are analyzed. Based on the characteristics of the type curves, seven flow regimes can be identified, including wellbore storage, transitional flow period, reservoir linear flow period, vertical pseudo-radial flow in fracture system, inter-porosity flow period, late-time pseudo-radial flow period, and the boundary-dominated flow period. Sensitivity analyses reveal that the penetration ratio of hydraulic fracture has primary influence on early-time transient pressure behavior and production contribution, while the stress sensitivity mainly affects the late-time transient pressure behavior. Gas production at the initial stage is mainly contributed by the high-pressure/high-permeability layer, and gas backflow will occur during initial production stage for obviously unequal initial formation pressures. Finally, two field cases are conducted to illustrate the applicability of the proposed model. The model and corresponding conclusions can provide technical support for performance analysis of tight gas reservoirs.

© 2025 The Authors. Publishing services by Elsevier B.V. on behalf of KeAi Communications Co. Ltd. This is an open access article under the CC BY-NC-ND license (http://creativecommons.org/licenses/by-nc-nd/4.0/).

1. Introduction

Tight gas, as one of the major unconventional gas resources, has become an important component of natural gas development in China (Zou et al., 2012; Jia, 2017). Tight sandstone gas reservoirs are usually characterized by strong heterogeneity, low porosity, and low permeability. Due to the ultra-low permeability of the tight formations, hydraulic fracturing is always applied to obtain commercial production of gas wells. Moreover, considering the low productivity of individual layer, co-production of multiple layers

E-mail addresses: guojingjing@swpu.edu.cn (J.-J. Guo), wanghaitao1999_@163.com (H.-T. Wang).

(commingled production) has become one of the important technologies to improve well performance in tight gas reservoirs (Chai et al., 2022; Wang et al., 2023).

Compared with the tight reservoirs in North America, most of the China's tight sandstone gas reservoirs are deposited in continental or transitional deposit facies (Jiang F.J. et al., 2023; Jiang L. et al., 2023; Zhang et al., 2020). The frequent migration and swing of rivers result in strong heterogeneity of reservoir properties, both vertically and laterally. The main tight gas reservoirs in China, such as Ordos Bain (Meng et al., 2016; Wang et al., 2024), Sichuan Basin (Guo et al., 2023), usually exhibit strong heterogeneity in reservoir properties. The physical properties of formations as well as the initial pressures of different layers can be quite different, which will lead to interlayer interference during the commingled production. The interlayer interference during multi-

^{*} Corresponding author.

^{**} Corresponding author.

layer coproduction mainly includes fluid flowing from highpressure layer into low-pressure layer though the wellbore, the inhibition of effective gas production from some layer, and the uneven recovery factor of different layers (Zhang et al., 2024; Liang et al., 2023). To efficiently and effectively exploit tight gas reservoirs, it is essential to accurately characterize the effect of interlayer heterogeneity on transient pressure behavior and production dynamics.

Lots of efforts have been done to characterize the transient pressure dynamics of multi-layer gas reservoirs. Early studies mainly concentrate on vertical wells, and various researchers proposed lots of analytical models to investigate the pressure transient behavior of vertical wells in multi-layer reservoirs, considering different initial conditions or boundary combinations. Lefkovits et al. (1961) investigated the transient pressure behavior of a completely penetrating vertical well in a bounded reservoir with several stratified layers, in which different layers were connected only at the wellbore. Gao et al. (1994) proposed a model to calculate the pressure drawdown response of a vertical well in a commingled production reservoir. The differences of formation properties, unequal layer radii and outer boundary condition were incorporated in Gao's model, while the unequal initial pressures of different layers were not taken into account. Based on the above models, a number of researchers have also proposed a variety of analytical solutions in the literature to describe the flowing problems in layered reservoirs with unequal initial pressures (Rahman and Matter, 2007; Lu et al., 2019; Shi et al., 2020a). Moreover, considering the lateral reservoir heterogeneity caused by artificial or natural processes, such as tectonic movements and reservoir stimulation, many researchers adopted composite model to analyze the pressure transient behavior of stratified reservoirs. Gomes and Ambastha (1993) developed an analytical model for multi-layered composite reservoirs, in which each layer was divided into two different zones, while the outer boundary of each layer was assumed to be the same. Shi et al. (2020b) adopted the composite model to describe the permeability heterogeneity caused by acid fracturing, and they proposed an analytical model to investigate the transient pressure behavior of gas wells in carbonate reservoir with multiple layers. However, the unequal layer radii were not taken into account in their model, either.

Due to the fact that the permeability of tight formations is always very low, the stimulation treatments such as acid fracturing and hydraulic fracturing are usually adopted to achieve commercial production (Liu et al., 2022; Zhang et al., 2023). Extensive research has been made to investigate the transient pressure dynamics of fractured wells in multilayer reservoirs. Shi (2021) summarized the seepage models published since 1960 for multilayered reservoirs. Among the 89 models, only 8 models were proposed for fractured wells considering commingled production of two or more layers. Osman (1993) was among the first to propose a series of mathematical models to analyze the transient behavior of fractured vertical well in a bounded reservoir with multiple layers. Based on this, various attempts have been made to capture the transient flowing behavior of fractured wells with commingled production. Manrique and Poe (2009) presented a procedure to optimize the productivity of fractured wells in stacked pay reservoirs based on the analysis of commingled production behavior of fractured wells in multilayer reservoirs. Sun et al. (2017) presented an analytical solution for fractured vertical wells in the three-layer reservoir, in which the pseudo-steady state crossflow between adjacent layers was taken into account, but only the mid-layer was hydraulically fractured in their model. More recently, Li et al. (2022) proposed a tri-linear flow model to investigate the behavior of fractured vertical wells in stratified reservoirs. However, the trilinear flow assumption is not valid in the radial flow regime. Wei et al. (2024) proposed a

semi-analytical model to investigate the transient pressure behavior of vertical wells with finite-conductivity hydraulic fracture in stratified reservoirs. The hydraulic fractures were assumed to fully penetrate the formation layer in their model, and the influences of fracture conductivity on transient pressure behavior were discussed. In sum, compared with analytical models of vertical wells in multi-layer reservoirs, the analytical or semi-analytical models of vertically fractured wells in multi-layered reservoirs are relatively limited.

Apart from the analytical and semi-analytical models, numerical simulation models are also adopted to investigate the multilayer co-production dynamics in gas reservoirs. Santiago et al. (2021) established a radial model to simulate the contribution of individual layer to the total production, in which the properties and dimensions of each layer varied within a given range. Their reservoir simulation results indicated that strong contrast in individual layer can lead to severe production inhibition of some layers because of interlayer interference. Chai et al. (2022) adopted a commercial numerical simulation software to simulate the production dynamics of multilayer co-production in tight gas reservoirs, and random forest method was employed to quantitatively figure out the primary influencing parameters of interference time and recovery factor. The simulation results revealed that the interlayer pressure difference has the most significant effect on the interference time and the recovery factor of each layer, while it has a relatively weak effect on the recovery factor of the gas reservoir under the condition of single gas-phase flow.

In recent years, extensive efforts have also been made on experimental characterization of interlayer interference during coproduction of multiple layers. Liu et al. (2020) and Tao et al. (2022) conducted several experiments with core samples collected from the Ordos Basin to evaluate the effects of pressure difference, physical property and production rate on the commingle production performance. A power-law relationship between the backflow time and the flow rate was found based on the analysis of experiment data. Wang et al. (2021) carried out a series of simultaneous and progressive production experiments with full-diameter cores to figure out the influence of interlayer interference. Experimental results indicated that progressive production of multiple layers could effectively avoid the occurrence of backflow, and thus the recovery factor of all layers could be improved. But larger interlayer pressure difference would lead to lower gas recovery in both simultaneous and progressive production. By considering the retention of the working fluid during drilling or fracturing, Ding et al. (2019) experimentally investigated the commingled production behavior of water-bearing cores. The experimental results confirmed that both gas and water back-flow from high-pressure layer to low-pressure layer occurred during commingled production, leading to a decrease in gas permeability in the near-wellbore area of the low-pressure lavers.

Laboratory experiment and theoretical method (including analytical models and numerical simulation methods) are generally adopted to characterize the interlayer interference and pressure dynamics during commingled production. Compared with the laboratory experiments, the primary advantage of theoretical method lies in its repeatability together with time saving. However, most of the pressure transient analysis models proposed in literature for multilayer reservoirs focused on vertical wells or fully penetrated fractured vertical wells, and very little work has been reported for fractured wells with limited fracture height. Actually, due to the complex in-situ stress states, the existence of natural fractures, and the changes in lithology, hydraulic fractures with limited fracture height may be generated during hydraulic fracturing in tight gas reservoirs (Scott et al., 2013). Yuan et al. (2013) investigated the geometry of the hydraulic fractures created in the upper Triassic

tight formation in the western Sichuan Basin in China. The petrophysical and geomechanical profiles of the target perforated interval indicate a fairly continuous and homogeneous sandstones by stable Gamma response, stable Young's modulus and Poisson's ratio. However, the vertical fracture height is limited to about 4.5 m based on the radioactive tracer log after stimulation. With the integrated analysis of data collected from various sources including cores. borehole image logs and so on, they concluded that the vertical hydraulic fracture with limited height mostly developed with the presence of low-angle bed-parallel features. Fan et al. (2020) further conducted a series of true tri-axial fracturing experiments to investigate the influence of complex in-situ stress state and natural fractures on hydraulic fracture geometry. Experimental results also validate that when the ratio of the overburden stress to the minimum horizontal stress is less than 1.2, and with the existence of preexisting low angle natural fracture, the vertical fracture with a limited height may form as a result. Another possible cause for limited hydraulic fracture height is the prevention of potential water invasion during production. For tight gas reservoirs with distributed aquifer zones or complex gas-water relationship, for example, the western and northern parts of Sulige Gas Field (Meng et al., 2016; Cheng et al., 2023), an artificial barrier was placed to control the vertical height of hydraulic fracture.

To understand the pressure transient behavior of vertical wells with limited fracture height in multi-layer gas reservoirs, a semi-analytical model is proposed in this work. The model takes into account the differences of formation properties, unequal initial pressures, different hydraulic fracture lengths and hydraulic fracture penetration ratios in each layer, as well as stress sensitivity. Point source function, Laplace transformation, Fourier transformation are adopted to obtain the semi-analytical solution of the presented model. The influences of prevailing factors, such as unequal initial formation pressure, unequal half-length of hydraulic fracture, penetration ratio of the hydraulic fracture, on the transient pressure behavior are discussed. Finally, two field cases are presented to verify the feasibility of the proposed model.

2. Physical model

Fig. 1 shows a schematic of a fractured vertical well in a multilayer tight gas reservoir. The gas reservoir contains M layers. A vertical well penetrates multiple layers, and each layer is stimulated by hydraulic fracturing. The height of the hydraulic fracture in layer j is h_{wj} , and the vertical midpoint of the hydraulic fracture in layer j is represented by z_{mj} . The commingled production of multiple layers is adopted, and the total production rate of the fractured well is constant.

Other corresponding assumptions are as follows.

- (1) Each layer is represented by dual-porosity media to account for the fracture network caused by hydraulic fracturing as well as natural fractures. Assuming that an impermeable barrier of a certain thickness exists between adjacent formation layers, and there is no crossflow between adjacent layers during production.
- (2) The physical properties are assumed to be homogeneous in each layer, while the physical properties are assumed to be different for different layers. Considering that tight gas reservoirs are generally characterized by tiny pores and complex pore-throat structures, gas flowing in tight formation is always subject to stress sensitivity, which may affect the transient pressure behavior. Therefore, the stress sensitivity of fracture system in each layer is taken into account.
- (3) The initial reservoir pressures of each layer can be different. The initial reservoir pressure of layer j is p_{ij} (j = 1, 2, ..., M).
- (4) The multi-layer reservoir is stimulated by separate layer fracturing. The properties of the hydraulic fracture in each layer, such as the fracture penetration height, fracture halflength, can be different. Moreover, the transverse fracture in each layer may not be parallel, which means there may be a certain angle between the hydraulic fractures in adjacent layers. The hydraulic fracture in each layer is assumed to be symmetrical with respect to the wellbore.
- (5) The hydraulic fracture is assumed to have infinite conductivity. The flux within each hydraulic fracture varies with location and production time. Gas flowing directly from the matrix to the wellbore is negligible.
- (6) Both the upper and lower boundaries of the reservoir are impermeable. The outer boundary of each layer is also assumed to be impermeable. The radius of the outer boundary of each layer can be different, and the outer boundary of layer j is r_{ej} (j = 1, 2, ..., M).
- (7) The reservoir is assumed to have uniform temperature. Gas flowing during the production is assumed to be isothermal flow, and it is assumed to conform to Darcy's law.
- (8) The fractured vertical well produces at a constant rate $q_{\rm sc}$, while the production rate of each layer is variable.
- (9) The gravity effect, capillary forces, and wellbore hydraulics are ignored. The skin factor in each layer can be different.

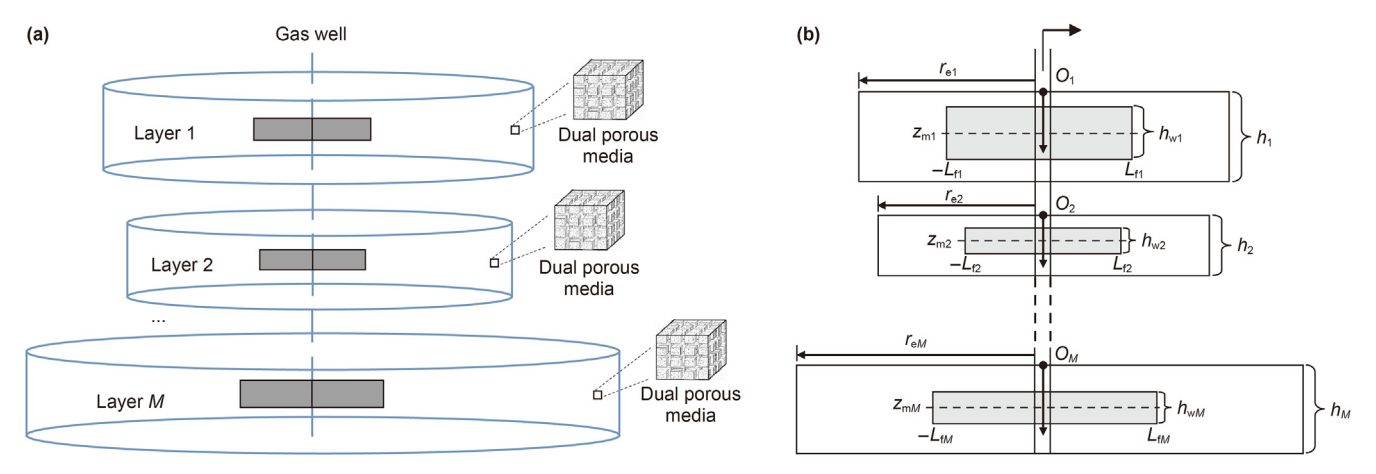


Fig. 1. Schematic of a fractured vertical well in a multilayer commingled dual porosity gas reservoir. (a) 3-dimensional view; (b) side view.

3. Mathematical model and solution

3.1. Point-sink solution in layer j

Assuming that a continuous point-sink is located at point (x_{wj}, y_{wj}, z_{wj}) in layer j in a multi-layer gas reservoir, and the production rate of the point sink under standard condition is $\hat{q}_j(t)$. By combining the continuity equation, motion equation, and

equation of state, the governing equations and corresponding initial and boundary conditions can be obtained, and the detailed derivation can be found in Appendix A. With the definitions of relevant dimensionless parameters shown in Table 1, we can obtain the dimensionless governing equations for a point-sink in layer j with consideration of stress sensitivity.

The dimensionless governing equation for natural fracture system is

$$\chi_{j} \left[\frac{\partial^{2} \psi_{\text{sfD}j}}{\partial r_{\text{D}j}^{2}} + \frac{1}{r_{\text{D}j}} \frac{\partial \psi_{\text{sfD}j}}{\partial r_{\text{D}j}} + L_{\text{fD}j}^{2} \frac{\partial^{2} \psi_{\text{sfD}j}}{\partial z_{\text{D}j}^{2}} - \gamma_{\text{D}j} \left(\frac{\partial \psi_{\text{sfD}j}}{\partial r_{\text{D}j}} \right)^{2} - \gamma_{\text{D}j} L_{\text{fD}j}^{2} \left(\frac{\partial \psi_{\text{sfD}j}}{\partial z_{\text{D}j}} \right)^{2} \right] \\
= L_{\text{fD}j}^{2} h_{\text{D}j}^{2} e^{\gamma_{\text{D}j}\psi_{\text{sfD}j}} \left[\omega_{j} \omega_{j}' \mu_{Rj} \frac{\partial \psi_{\text{sfD}j}}{\partial t_{\text{D}}} + \chi_{j} \lambda_{j} \left(\psi_{\text{sfD}j} - \psi_{\text{smD}j} \right) \right] \tag{1}$$

Table 1
Definitions of dimensionless parameters

| Table 1 Definitions of dimensionless parameters. | |
|--|--|
| Dimensionless parameter | Definition |
| Dimensionless pseudo-pressure of the natural fracture system in layer j (based on the initial pseudo-pressure of layer ψ_{ij}) | $\dot{\mathbf{j}}, \psi_{sffb,i} = \frac{\pi (k_{fh} h)_{t} T_{sc}}{\pi} (\psi_{li} - \psi_{fi})$ |
| ψ_{ij}) Dimensionless pseudo-pressure of the matrix system in layer j (based on the initial pseudo-pressure of layer j , ψ_{ij}) | $\psi_{\text{smD}j} = \frac{p_{\text{sc}}q_{\text{sc}}I}{m_{\text{cc}}q_{\text{sc}}T} (\psi_{\text{lj}} - \psi_{\text{mj}})$ |
| Dimensionless wellbore pseudo-pressure in layer j (based on the initial pseudo-pressure of layer j , ψ_{lj}) | $\psi_{\text{swD}j} = \frac{\pi (k_{\text{fh}} h)_{\text{t}} T_{\text{sc}}}{p_{\text{sc}} q_{\text{sc}} T} (\psi_{\text{l}j} - \psi_{\text{w}j})$ |
| Dimensionless pseudo-pressure of the natural fracture system in layer j (based on the reference pseudo-pressure, ψ_r) | $\psi_{\text{fD}j} = \frac{\pi (k_{\text{fh}} h)_{\text{t}} T_{\text{sc}}}{p_{\text{sc}} q_{\text{sc}} T} (\psi_{\text{r}} - \psi_{\text{f}j}) \text{ with } \psi_{\text{r}} = \max(\psi_{\text{l}j})$ |
| Dimensionless pseudo-pressure of the matrix system in layer j (based on the reference pseudo-pressure, $\psi_{\rm r}$) | $\psi_{\text{mD}j} = \frac{\pi (k_{\text{fh}} h)_{\text{t}} T_{\text{sc}}}{p_{\text{sc}} q_{\text{sc}} T} (\psi_{\text{r}} - \psi_{\text{m}j})$ |
| Dimensionless wellbore pseudo-pressure in layer j (based on the reference pseudo-pressure, ψ_{r}) | $\psi_{\text{wD}j} = \frac{\pi (k_{\text{fh}} h)_{\text{t}} T_{\text{sc}}}{p_{\text{sc}} q_{\text{sc}} T} (\psi_{\text{r}} - \psi_{\text{w}j})$ |
| Dimensionless initial pressure in layer j (based on the reference pseudo-pressure, $\psi_{\rm r}$) | $\psi_{\text{ID}j} = \frac{\pi (k_{\text{fh}} h)_{\text{t}} T_{\text{sc}}}{n_{\text{sc}} q_{\text{sc}} T} (\psi_{\text{r}} - \psi_{\text{l}j})$ |
| Dimensionless permeability modulus | $\gamma_{Dj} = \beta_j \frac{p_{sc}q_{sc}T}{\pi(k_{Pl}h)_{t}T_{sc}}$ |
| Dimensionless distance of x -, y - and z -coordinates in layer j | $x_{Di} = x_i/L_{fi}, y_{Di} = y_i/L_{fi}, z_{Di} = z_i/h_i$ |
| Dimensionless z -coordinate of the point-sink in layer j | $z_{wDj} = z_{wj}/h_j$ |
| Dimensionless z -coordinate of the vertical midpoint of the hydraulic fracture in layer j | $z_{\mathrm{mD}j} = z_{\mathrm{m}j}/h_j$ |
| Dimensionless radial distance in layer j | $r_{\rm Dj} = \frac{r_j}{L_{\rm Fi}}, r_j = \sqrt{(x_j - x_{\rm Wj})^2 + (y_j - y_{\rm Wj})^2}$ |
| Dimensionless radial infinitesimal variable in layer <i>j</i> | $\sigma_{\mathrm{D}i} = \sigma_i/L_{\mathrm{f}i}$ |
| Dimensionless vertical infinitesimal variable in layer <i>j</i> | $arepsilon_{\mathrm{D}i} = arepsilon_i / L_{\mathrm{f}i}$ |
| Dimensionless length of hydraulic fracture in layer j | · · · · |
| | $L_{	ext{fD}j} = rac{L_{	ext{f}j}}{h_j} \sqrt{rac{k_{	ext{fv}j0}}{k_{	ext{fh}j0}}}$ |
| Dimensionless formation thickness of layer j | $h_{\mathrm{D}j} = rac{h_{j}}{r_{\mathrm{w}}} \sqrt{rac{k_{\mathrm{fh}j0}}{k_{\mathrm{fv}i0}}}$ |
| Discovering the state of the st | V3- |
| Dimensionless perforated formation thickness of layer j | $h_{\mathrm{WD}j} = \frac{h_{\mathrm{W}j}}{r_{\mathrm{W}}} \sqrt{\frac{k_{\mathrm{fh}j0}}{k_{\mathrm{fv}j0}}}$ |
| Dimensionless time | $t_{\rm D} = \frac{(k_{\rm fh}h)_{\rm t}t}{[(\phi_{\rm f}hC_{\rm f})_{\rm t} + (\phi_{\rm m}hC_{\rm m})_{\rm t}]\mu_{\rm l1}r_{\rm w}^{2}}$ |
| Dimensionless production rate of the point-sink in layer <i>j</i> | $\widehat{q}_{\mathrm{D}i} = \widehat{q}_{\mathrm{D}i}(t_{\mathrm{D}}) + (\varphi_{\mathrm{m}} n_{\mathrm{C}_{\mathrm{m}}})_{\mathrm{t}} \mu_{\mathrm{I}1} n_{\mathrm{W}}^{2}$ |
| Formation coefficient ratio of layer <i>j</i> among multiple layers | |
| | $\chi_j = \frac{k_{\text{fh}j0}h_j}{(k_{\text{fh}}h)_{\text{t}}} \text{ with } (k_{\text{fh}}h)_{\text{t}} = \sum_{j=1}^{M} k_{\text{fh}j0}h_j$ |
| Storativity ratio of natural fracture system of layer j | $\omega_j = \frac{\phi_{fj} h_j C_{fj}}{\phi_{fj} h_j C_{fj} + \phi_{mj} h_j C_{mj}}$ |
| Storativity ratio of layer <i>j</i> among multiple layers | |
| Storauvity ratio of rayer y among muniple rayers | $\omega_{j}^{'} = \frac{\phi_{fj}h_{j}C_{fj+}\phi_{mj}h_{j}C_{mj}}{\left(\phi_{f}hC_{f}\right)_{t} + \left(\phi_{m}hC_{m}\right)_{t}}$ |
| | with $(\phi_f h C_f)_t = \sum_{j=1}^M \phi_{fj} h_j C_{fj}$, |
| | $(\phi_{\mathbf{m}}hC_{\mathbf{m}})_{\mathbf{t}} = \sum_{j=1}^{M} \phi_{\mathbf{m}j}h_{j}C_{\mathbf{m}j}$ |
| Inter-porosity flowing coefficient of layer j | $\alpha_j k_{mj} r_w^2$ |
| | $\lambda_j = \frac{\alpha_j k_{mj} r_w^2}{k_{fhj0}}$ |
| Gas viscosity ratio | $\mu_{\rm Rj} = \frac{\mu_{\rm lj}}{\mu_{\rm rs}}$ |
| | ' N |

The dimensionless governing equation for matrix system is

$$(1 - \omega_j)\omega_j'\mu_{Rj}\frac{\partial \psi_{smDj}}{\partial t_D} - \chi_j\lambda_j(\psi_{sfDj} - \psi_{smDj}) = 0$$
 (2)

Corresponding initial conditions are as follows:

$$\psi_{\text{sfD}j}(r_{\text{D}j}, z_{\text{D}j}, t_{\text{D}})\Big|_{t_{\text{b}}=0} = 0$$
 (3)

$$\psi_{\text{smD}j}(r_{\text{D}j}, z_{\text{D}j}, t_{\text{D}})|_{t_{\text{D}}=0} = 0$$
 (4)

The impermeable lateral, upper and lower boundary conditions of layer i are given as

$$\left. \frac{\partial \psi_{\text{sfD}j}(r_{\text{D}j}, z_{\text{D}j}, t_{\text{D}})}{\partial r_{\text{D}j}} \right|_{r_{\text{D}j} = r_{\text{eD}j}} = 0 \tag{5}$$

$$\left. \frac{\partial \psi_{\text{sfD}j}(r_{\text{D}j}, z_{\text{D}j}, t_{\text{D}})}{\partial z_{\text{D}j}} \right|_{z_{\text{D}i}=0} = 0 \tag{6}$$

$$\left. \frac{\partial \psi_{\text{sfD}j}(r_{\text{D}j}, z_{\text{D}j}, t_{\text{D}})}{\partial z_{\text{D}j}} \right|_{z_{\text{D}j}=1} = 0 \tag{7}$$

Given that the production rate of the continuous point-sink is $\widehat{q}_j(t)$, the inner boundary condition can be expressed as

$$\begin{split} &\lim_{\epsilon_{Dj}\to 0}\int\limits_{z_{wDj}-\epsilon_{Dj}/2}^{z_{wDj}+\epsilon_{Dj}/2}\left[\lim_{\sigma_{Dj}\to 0}\left(\chi_{j}r_{Dj}e^{-\gamma_{Dj}\psi_{sfDj}}\frac{\partial\psi_{sfDj}}{\partial r_{Dj}}\right)_{r_{Dj}=\sigma_{Dj}}\right]dz_{Dj} = \\ &-\widehat{q}_{Dj}(t_{D}) \end{split} \tag{8}$$

Due to the strong nonlinearity caused by consideration of stress sensitivity, it is difficult to obtain the analytical solution for the above continuous point-sink model. The Pedrosa's transformation is introduced to linearize the above model.

$$\psi_{\text{sfD}j}(r_{\text{D}j}, t_{\text{D}}) = -\frac{1}{\gamma_{\text{D}j}} \ln \left[1 - \gamma_{\text{D}j} \xi_{\text{sfD}j}(r_{\text{D}j}, t_{\text{D}}) \right]$$
 (9)

in which ξ_{sfDj} can be expanded as the following power series in the parameter γ_{Dj} :

$$\xi_{\text{sfD}j} = \xi_{\text{sfD}j0} + \gamma_{\text{D}j}\xi_{\text{sfD}j1} + \gamma_{\text{D}j}^2\xi_{\text{sfD}j2} + \cdots$$
 (10)

where ξ_{sfDj0} , ξ_{sfDj1} , and ξ_{sfDj2} are the zero-order, first-order, and second-order approximations of ξ_{sfDj} .

The corresponding terms $\frac{1}{1-\gamma_{\mathrm{D}j}\xi_{\mathrm{sfD}j}}$ and $-\frac{1}{\gamma_{\mathrm{D}j}}\ln[1-\gamma_{\mathrm{D}j}\xi_{\mathrm{sfD}j}]$ can be also expanded with respect to $\gamma_{\mathrm{D}j}$ as follows:

$$\frac{1}{1 - \gamma_{Dj}\xi_{sfDj}} = 1 + \gamma_{Dj}\xi_{sfDj} + \gamma_{Dj}^2\xi_{sfDj}^2 + \cdots$$
(11)

$$-\frac{1}{\gamma_{Dj}}\ln\left[1-\gamma_{Dj}\xi_{sfDj}\right] = \xi_{sfDj} + \frac{1}{2}\gamma_{Dj}\xi_{sfDj}^{2} + \cdots$$
 (12)

Considering the small value of dimensionless permeability modulus, γ_{Dj} , a zero-order approximate solution can meet the practical accuracy requirement (Zhang and Yang, 2021).

Therefore, the governing equations for natural fracture and matrix systems, i.e., Eqs. (1) and (2), can be transformed into the

following forms:

$$\chi_{j} \left\{ \frac{\partial^{2} \xi_{\text{sfD}j0}}{\partial r_{\text{D}j}^{2}} + \frac{1}{r_{\text{D}j}} \frac{\partial \xi_{\text{sfD}j0}}{\partial r_{\text{D}j}} + L_{\text{fD}j}^{2} \frac{\partial^{2} \xi_{\text{sfD}j0}}{\partial z_{\text{D}j}^{2}} \right\} \\
= L_{\text{fD}j}^{2} h_{\text{D}j}^{2} \left\{ \omega_{j} \omega_{j}^{\prime} \mu_{\text{R}j} \frac{\partial \xi_{\text{sfD}j0}}{\partial t_{\text{D}}} + \chi_{j} \lambda_{j} \left(\xi_{\text{sfD}j0} - \psi_{\text{smD}j} \right) \right\}$$
(13)

$$(1 - \omega_j)\omega_j'\mu_{Rj} \frac{\partial \psi_{\text{smD}j}}{\partial t_D} - \chi_j \lambda_j \left(\xi_{\text{sfD}j0} - \psi_{\text{smD}j}\right) = 0$$
 (14)

The initial and boundary conditions become

$$\left. \xi_{\text{sfD}j0}(r_{\text{D}j}, z_{\text{D}j}, t_{\text{D}}) \right|_{t_{\text{D}}=0} = 0$$
 (15)

$$\psi_{\text{smD}j}(r_{\text{D}j}, z_{\text{D}j}, t_{\text{D}})\big|_{t_{\text{D}}=0} = 0 \tag{16}$$

$$\left. \frac{\partial \xi_{\text{sfD}j0} \left(r_{\text{D}j}, z_{\text{D}j}, t_{\text{D}} \right)}{\partial r_{\text{D}j}} \right|_{r_{\text{D}j} = r_{\text{eD}j}} = 0 \tag{17}$$

$$\left. \frac{\partial \xi_{\text{sfD}j0}(r_{\text{D}j}, z_{\text{D}j}, t_{\text{D}})}{\partial z_{\text{D}j}} \right|_{z_{\text{D}i}=0} = 0 \tag{18}$$

$$\left. \frac{\partial \xi_{sfDj0}(r_{Dj}, z_{Dj}, t_D)}{\partial z_{Dj}} \right|_{z_{Di}=1} = 0 \tag{19}$$

$$\lim_{\varepsilon_{\rm Dj}\to 0} \int_{z_{\rm wDj}-\varepsilon_{\rm Dj}/2}^{z_{\rm wDj}+\varepsilon_{\rm Dj}/2} \left[\lim_{\sigma_{\rm Dj}\to 0} \left(\chi_j r_{\rm Dj} \frac{\partial \xi_{\rm sfDj0}}{\partial r_{\rm Dj}} \right)_{r_{\rm Dj}=\sigma_{\rm Dj}} \right] dz_{\rm Dj} = - \widehat{q}_{\rm Dj}(t_{\rm D})$$
(20)

Performing the Laplace transformation with respect to $t_{\rm D}$ and Fourier finite cosine integral transformation with respect to $z_{\rm D}$ on Eqs. (13)–(20), and followed by Ozkan and Raghavan (1991), we can obtain the solution of point-sink in layer j in the Laplace-Fourier domain as follows:

$$\widetilde{\overline{\xi}}_{sfDj0}(r_{Dj}, n, s) = \frac{\overline{\widehat{q}}_{Dj}(s)}{\chi_{j}} \cos(n\pi z_{wDj})$$

$$\times \left[K_{0}(\alpha_{n,j}r_{Dj}) + \frac{K_{1}(\alpha_{n,j}r_{eDj})}{I_{1}(\alpha_{n,j}r_{eDj})} I_{0}(\alpha_{n,j}r_{Dj}) \right]$$
(21)

where s is the Laplace transformation variable, dimensionless; $\overline{*}$ represent the Laplace transformation of parameter *; $\overset{\sim}{*}$ represent the Fourier finite cosine transformation of parameter *; $\alpha_{n,j} = \sqrt{sf(s) + n^2\pi^2L_{\mathrm{fD}j}^2}$ $(n=0,\ 1,\ 2,\ \cdots)$, and the expression of f(s) is given as

$$f(s) = \frac{\omega_j' \mu_{Rj} h_{Dj}^2 L_{fDj}^2 \chi_j \lambda_j + s \omega_j (1 - \omega_j) {\omega_j'}^2 \mu_{Rj}^2 h_{Dj}^2 L_{fDj}^2}{\chi_j \left[s (1 - \omega_j) \omega_j' \mu_{Rj} + \chi_j \lambda_j \right]}$$
(22)

Performing inverse Fourier finite cosine integral transformation on Eq. (21), we can obtain the basic point-sink solution of layer j in the multi-layer dual porosity reservoir in the Laplace domain as follows:

$$\overline{\xi}_{sfDj0} = \frac{\overline{\widehat{q}}_{Dj}(s)}{\chi_{j}} \begin{bmatrix} K_{0}(\alpha_{0,j}r_{Dj}) + \frac{K_{1}(\alpha_{0,j}r_{eDj})}{I_{1}(\alpha_{0,j}r_{eDj})} I_{0}(\alpha_{0,j}r_{Dj}) + 2\sum_{n=1}^{\infty} K_{0}(\alpha_{n,j}r_{Dj}) \cos(n\pi z_{Dj}) \cos(n\pi z_{WDj}) \\ +2\sum_{n=1}^{\infty} \frac{K_{1}(\alpha_{n,j}r_{eDj})}{I_{1}(\alpha_{n,j}r_{eDj})} I_{0}(\alpha_{n,j}r_{Dj}) \cos(n\pi z_{WDj}) \end{bmatrix}$$
(23)

3.2. Line-sink solution in layer j

Based on the superposition principle, the line-sink solution of layer j in the multi-layer reservoir incorporating stress sensitivity effect can be obtained by integrating the basic point-sink solution (Eq. (23)) along the perforation part, which is

3.3. Transient pressure solution of the multi-layer reservoir

Based on the superposition principle, the transient pressure caused by the hydraulic fracture in layer j can be obtained by integrating Eq. (25) along the hydraulic fracture with respect to x_{wj} from $-L_{fj}$ to L_{fj} .

$$\bar{\xi}_{sfDj0} = \int_{z_{mj} - \frac{h_{wj}}{2}}^{z_{mj} + \frac{h_{wj}}{2}} \frac{q_{j}(s) / h_{wj}}{q_{sc}\chi_{j}} + 2 \sum_{n=1}^{\infty} K_{0}(\alpha_{n,j}r_{Dj}) \cos(n\pi z_{wDj}) \log(\alpha_{n,j}r_{Dj}) dz_{wDj} dz_{wj} + 2 \sum_{n=1}^{\infty} K_{0}(\alpha_{n,j}r_{eDj}) \cos(n\pi z_{wDj}) \cos(n\pi z_{wDj}) dz_{wj}$$

$$+ 2 \sum_{n=1}^{\infty} \frac{K_{1}(\alpha_{n,j}r_{eDj})}{I_{1}(\alpha_{n,j}r_{eDj})} I_{0}(\alpha_{n,j}r_{Dj}) \cos(n\pi z_{wDj}) dz_{wj}$$
(24)

where $\overline{q_j}(s)$ is the Laplace transformation of $q_j(s)$, and $q_j(s)$ is the production rate of the line-sink in layer j, m^3/s .

With some mathematical simplification, Eq. (24) can be written

$$\overline{\xi}_{sfDj0} = \frac{\overline{q_{j}(s)}}{q_{sc}\chi_{j}} \begin{bmatrix}
K_{0}(\alpha_{0,j}r_{Dj}) + \frac{K_{1}(\alpha_{0,j}r_{eDj})}{I_{1}(\alpha_{0,j}r_{eDj})}I_{0}(\alpha_{0,j}r_{Dj}) \\
+ \frac{4h_{Dj}}{\pi h_{wDj}} \sum_{n=1}^{\infty} \frac{1}{n}K_{0}(\alpha_{n,j}r_{Dj})\cos\left(n\pi z_{Dj}\right)\cos\left(n\pi z_{mDj}\right)\sin\left(n\pi \frac{h_{wDj}}{2h_{Dj}}\right) \\
+ \frac{4h_{Dj}}{\pi h_{wDj}} \sum_{n=1}^{\infty} \frac{1}{n} \frac{K_{1}(\alpha_{n,j}r_{eDj})}{I_{1}(\alpha_{n,j}r_{eDj})}I_{0}(\alpha_{n,j}r_{Dj})\cos\left(n\pi z_{Dj}\right)\cos\left(n\pi z_{mDj}\right)\sin\left(n\pi \frac{h_{wDj}}{2h_{Dj}}\right)
\end{bmatrix}$$
(25)

Eq. (25) is the basic zero-order line-sink solution of layer j in the multi-layer dual porosity reservoir in the Laplace domain.

$$\overline{\xi}_{sfDj0} = \int_{-L_{ij}}^{L_{ij}} \frac{\overline{q}_{fj}(x_{wj}, s)}{q_{sc}\chi_{j}} \begin{bmatrix} K_{0}(\alpha_{0,j}r_{Dj}) + \frac{K_{1}(\alpha_{0,j}r_{eDj})}{I_{1}(\alpha_{0,j}r_{eDj})} I_{0}(\alpha_{0,j}r_{Dj}) \\ + \frac{4h_{j}}{\pi h_{wj}} \sum_{n=1}^{\infty} \frac{1}{n} K_{0}(\alpha_{n,j}r_{Dj}) \cos\left(n\pi z_{Dj}\right) \cos\left(n\pi z_{mDj}\right) \sin\left(n\pi \frac{h_{wj}}{2h_{j}}\right) \\ + \frac{4h_{j}}{\pi h_{wj}} \sum_{n=1}^{\infty} \frac{1}{n} \frac{K_{1}(\alpha_{n,j}r_{eDj})}{I_{1}(\alpha_{n,j}r_{eDj})} I_{0}(\alpha_{n,j}r_{Dj}) \cos\left(n\pi z_{Dj}\right) \cos\left(n\pi z_{mDj}\right) \sin\left(n\pi \frac{h_{wj}}{2h_{j}}\right) \end{bmatrix} dx_{wj} \tag{26}$$

where $\overline{q}_{fj}(x_{wj},s)$ is the Laplace transformation of $q_{fj}(x_{wj},t)$; $q_{fj}(x_{wj},t)$ is the flux density of the hydraulic fracture in layer j, $m^3/(m\cdot s)$; $r_{Dj}=\sqrt{(x_{Dj}-x_{wDj})^2+(y_{Dj}-y_{wDj})^2}$.

Since the bottomhole pressure or the pressure along the hydraulic fracture is the parameter of interest in the pressure transient analysis of gas wells, thus we can set $y_{Dj} = y_{wDj}$. Then by introducing the following dimensionless flux density

$$\overline{q}_{\text{fD}j}(s) = \frac{2\overline{q}_{\text{fj}}(s)L_{\text{fj}}}{q_{\text{sc}}} \tag{27}$$

and with the assumption of infinite-conductivity hydraulic fracture, Eq. (26) can be written as

Eq. (29) represents the zero-order approximation of the dimensionless pseudo-pressure response caused by the hydraulic fracture in layer j. It is noted that $\overline{q}_{fDj}(x_{wDj},s)$ is a function of x_{wDj} in the Laplace domain, which cannot be analytically solved.

Following Gringarten et al. (1974) and Wang (2014), the method of discretization of hydraulic fractures is adopted to obtain the semi-analytical solution of Eq. (29). As illustrated in Fig. 2, the hydraulic fracture in each layer is discretized into N discrete segments. The dimensionless length of each segment is $\Delta x_D = 1/N$. When the number of the discrete segments is large enough, it is reasonable to assume that the flux of each fracture segment is uniform.

With the discretization of the hydraulic fracture in layer j, Eq. (29) can then be written as

$$\overline{\xi}_{sfDj0} = \frac{1}{2\chi_{j}} \int_{-1}^{1} \overline{q}_{fDj}(x_{wDj}, s) \begin{cases} K_{0}(\alpha_{0,j}|x_{Dj} - x_{wDj}|) + \frac{K_{1}(\alpha_{0,j}r_{eDj})}{I_{1}(\alpha_{0,j}r_{eDj})} I_{0}(\alpha_{0,j}|x_{Dj} - x_{wDj}|) \\ + \frac{4h_{j}}{\pi h_{wj}} \sum_{n=1}^{\infty} \frac{1}{n} K_{0}(\alpha_{n,j}|x_{Dj} - x_{wDj}|) \cos\left(n\pi z_{Dj}\right) \cos\left(n\pi z_{mDj}\right) \sin\left(n\pi \frac{h_{wj}}{2h_{j}}\right) \\ + \frac{4h_{j}}{\pi h_{wj}} \sum_{n=1}^{\infty} \frac{1}{n} \frac{K_{1}(\alpha_{n,j}r_{eDj})}{I_{1}(\alpha_{n,j}r_{eDj})} I_{0}(\alpha_{n,j}|x_{Dj} - x_{wDj}|) \cos\left(n\pi z_{Dj}\right) \cos\left(n\pi z_{mDj}\right) \sin\left(n\pi \frac{h_{wj}}{2h_{j}}\right) \end{cases}$$

$$(28)$$

Since in the same layer, the hydraulic fracture is symmetrical with respect to the wellbore, the flux density of the hydraulic fracture is also symmetrical with respect to the wellbore. Eq. (28) thus can be further written as

$$\begin{split} \overline{\xi}_{sfDj0} &= \frac{1}{2\chi_{j}} \cdot \int\limits_{0}^{1} \overline{q}_{fDj}(x_{wDj}, s) \\ &\times \begin{cases} K_{0}(\alpha_{0,j}|x_{Dj} + x_{wDj}|) + K_{0}(\alpha_{0,j}|x_{Dj} - x_{wDj}|) \\ + \frac{K_{1}(\alpha_{0,j}r_{eDj})}{I_{1}(\alpha_{0,j}r_{eDj})} I_{0}(\alpha_{0,j}|x_{Dj} + x_{wDj}|) + \frac{K_{1}(\alpha_{0,j}r_{eDj})}{I_{1}(\alpha_{0,j}r_{eDj})} I_{0}(\alpha_{0,j}|x_{Dj} - x_{wDj}|) \\ \times \left\{ + \frac{4h_{j}}{\pi h_{wj}} \sum_{n=1}^{\infty} \frac{1}{n} \left[K_{0}(\alpha_{n,j}|x_{Dj} + x_{wDj}|) + K_{0}(\alpha_{n,j}|x_{Dj} - x_{wDj}|) \right] \cos\left(n\pi z_{Dj}\right) \cos\left(n\pi z_{Dj}\right) \sin\left(n\pi \frac{h_{wj}}{2h_{j}}\right) \\ + \frac{4h_{j}}{\pi h_{wj}} \sum_{n=1}^{\infty} \frac{1}{n} \left[\frac{K_{1}(\alpha_{n,j}r_{eDj})}{I_{1}(\alpha_{n,j}r_{eDj})} I_{0}(\alpha_{n,j}|x_{Dj} + x_{wDj}|) + \frac{K_{1}(\alpha_{n,j}r_{eDj})}{I_{1}(\alpha_{n,j}r_{eDj})} I_{0}(\alpha_{n,j}|x_{Dj} - x_{wDj}|) \right] \cos\left(n\pi z_{Dj}\right) \cos\left(n\pi z_{Dj}\right) \cos\left(n\pi z_{Dj}\right) \sin\left(n\pi \frac{h_{wj}}{2h_{j}}\right) \end{cases} \end{split}$$

$$\overline{\xi}_{sfDj0}(x_{Dj}, 0, z_{mDj}) = \frac{1}{2\chi_{j}} \cdot \sum_{i=1}^{N} \overline{q}_{fDij}(s)$$

$$= \frac{1}{2\chi_{j}} \cdot \sum_{i=1}^{N} \overline{q}_{fDij}(s)$$

$$+ \frac{K_{0}(\alpha_{0j}|x_{Dj} + x_{wDj}|) + K_{0}(\alpha_{0j}|x_{Dj} - x_{wDj}|)}{I_{1}(\alpha_{0j}r_{eDj})} I_{0}(\alpha_{0j}|x_{Dj} + x_{wDj}|) + \frac{K_{1}(\alpha_{0j}r_{eDj})}{I_{1}(\alpha_{0j}r_{eDj})} I_{0}(\alpha_{0j}|x_{Dj} - x_{wDj}|)$$

$$+ \frac{4h_{j}}{\pi h_{wj}} \sum_{n=1}^{\infty} \frac{1}{n} \left[K_{0}(\alpha_{nj}|x_{Dj} + x_{wDj}|) + K_{0}(\alpha_{nj}|x_{Dj} - x_{wDj}|) \right] \cos\left(n\pi z_{Dj}\right) \cos\left(n\pi z_{Dj}\right) \sin\left(n\pi \frac{h_{wj}}{2h_{j}}\right)$$

$$+ \frac{4h_{j}}{\pi h_{wj}} \sum_{n=1}^{\infty} \frac{1}{n} \left[\frac{K_{1}(\alpha_{nj}r_{eDj})}{I_{1}(\alpha_{nj}r_{eDj})} I_{0}(\alpha_{nj}|x_{Dj} + x_{wDj}|) + \frac{K_{1}(\alpha_{nj}r_{eDj})}{I_{1}(\alpha_{nj}r_{eDj})} I_{0}(\alpha_{nj}|x_{Dj} - x_{wDj}|) \right] \cos\left(n\pi z_{Dj}\right) \cos\left(n\pi z_{Dj}\right) \cos\left(n\pi z_{Dj}\right) \sin\left(n\pi \frac{h_{wj}}{2h_{j}}\right)$$

$$(30)$$

where $\overline{q}_{\text{fD}i,j}(s)$ is the Laplace transformation of $q_{\text{fD}i,j}(t)$; and $q_{\text{fD}i,j}(t)$ is the dimensionless flux of fracture segment i in layer j.

Since the conductivity of the hydraulic fracture is assumed to be infinitely large, the dimensionless wellbore pseudo-pressure is equal to the dimensionless pressure along the hydraulic fracture, which gives

$$\overline{\xi}_{\text{sfDi0}}(\widehat{x}_{\text{D}k,j},0,z_{\text{mDj}}) = \overline{\xi}_{\text{swDj0}}, \quad k = 1, 2, 3, \dots, N$$
(31)

where $\overline{\xi}_{\text{swDj0}}$ is the Laplace transformation of ξ_{swDj0} ; ξ_{swDj0} is the zero-order approximation of the dimensionless wellbore pseudopressure defined based on the initial pseudo-pressure of layer j; $\widehat{x}_{Dk,j}$ is the dimensionless x-coordinate of fracture segment k in layer j.

Combination of Eqs. (30) and (31) yields

The subscript k in Eq. (32) represents the kth (k = 1, 2, 3, ..., N) discrete segment in the hydraulic fracture, while the subscript j represents layer j (j = 1, 2, 3, ..., M). By writing Eq. (32) for all fracture segments, we can obtain $M \times N$ equations. However, the number of unknowns, which are $\overline{q}_{\text{fD}i,j}(s)$ and $\overline{\xi}_{\text{swD}j0}$ (i = 1, 2, 3, ..., N; j = 1, 2, 3, ..., M), is $M \times N + M$. Additional equations are required to successfully solve the problem.

It should be addressed that $\xi_{\mathrm{swD}j0}$ in Eq. (32) is the zero-order approximation of $\psi_{\mathrm{swD}j}$, and $\psi_{\mathrm{swD}j}$ is defined based on the initial reservoir pressure of layer j. As the initial pressures of different layers can be different, the expressions of $\psi_{\mathrm{swD}j}$ for different layers are actually different. To ensure that each individual layer has the same expression of dimensionless pressure, $\psi_{\mathrm{wD}j}$, which is defined based on the unified initial reservoir pressure, is introduced.

According to the definitions of $\psi_{\text{SWD}j}$ and $\psi_{\text{WD}j}$ shown in Table 1, the following equation can be obtained

$$\overline{\xi}_{swDj0} = \frac{1}{2\chi_{j}} \cdot \sum_{i=1}^{N} \overline{q}_{fDij}(s)$$

$$= \frac{1}{1} \cdot \left[\frac{K_{1}(\alpha_{0,j}r_{eDj})}{K_{1}(\alpha_{0,j}r_{eDj})} I_{0}(\alpha_{0,j} | \widehat{x}_{Dk,j} - x_{wDj} |) \right] cos(n\pi z_{Dj}) co$$

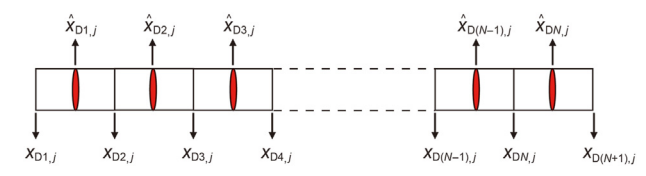


Fig. 2. Schematic of discretization of the hydraulic fracture in layer *j*.

$$\psi_{\text{WD}i} = \psi_{\text{ID}i} + \psi_{\text{SWD}i} \tag{33}$$

where $\psi_{\text{ID}j}$ is the dimensionless initial pseudo-pressure of layer j, and its expression is given in Table 1.

Taking into account the effect of skin factor in layer j, Eq. (33) can be further written as

$$\psi_{\text{WD}i} = \psi_{\text{ID}i} + \psi_{\text{SWD}i} + S_i \tag{34}$$

Since the wellbore hydraulic is ignored, the wellbore pseudopressures in different layers are identical, which yields

$$\psi_{\text{wD1}} = \psi_{\text{wD2}} = \psi_{\text{wD3}} = \dots = \psi_{\text{wDM}}$$
 (35)

Combination of Eqs. (34) and (35) yields

$$\psi_{\text{ID1}} + \psi_{\text{swD1}} + S_1 = \psi_{\text{ID2}} + \psi_{\text{swD2}} + S_2 = \psi_{\text{ID3}} + \psi_{\text{swD3}} + S_3 = \dots$$

$$= \psi_{\text{IDM}} + \psi_{\text{swDM}} + S_M$$
(36)

Performing the Laplace transformation on Eq. (36), we can have

$$\frac{\psi_{\text{ID1}} + S_1}{s} + \overline{\psi}_{\text{swD1}} = \frac{\psi_{\text{ID2}} + S_2}{s} + \overline{\psi}_{\text{swD2}} = \frac{\psi_{\text{ID3}} + S_3}{s} + \overline{\psi}_{\text{swD3}} = \dots$$

$$= \frac{\psi_{\text{IDM}} + S_M}{s} + \overline{\psi}_{\text{swDM}}$$
(37a)

Thus the zero-order approximation of Eq. (37a) can be written as

$$\frac{\psi_{\text{ID1}} + S_{1}}{s} + \overline{\xi}_{\text{swD1},0} = \frac{\psi_{\text{ID2}} + S_{2}}{s} + \overline{\xi}_{\text{swD2},0} = \frac{\psi_{\text{ID3}} + S_{3}}{s} + \overline{\xi}_{\text{swD3},0}$$

$$= \dots = \frac{\psi_{\text{IDM}} + S_{M}}{s} + \overline{\xi}_{\text{swDM},0}$$
(37b)

In addition, the constant production rate constraint of the gas well should be always satisfied

$$1 = \sum_{j=1}^{M} \sum_{i=1}^{N} q_{fDi,j} \Delta L_{fDj}$$
 (38)

where $q_{\text{fD}i,j}$ is the dimensionless flux density of the *i*th fracture segment in layer j, i.e., the discrete segment (i, j), which is defined by Eq. (39); $\Delta L_{\text{fD}j}$ is the dimensionless length of the discrete segment (i, j), which is defined by Eq. (40).

$$q_{\text{fD}i,j} = \frac{2q_{\text{f}i,j}L_{\text{f}j}}{q_{\text{sc}}} \tag{39}$$

$$\Delta L_{\text{fD}j} = \frac{\Delta L_{\text{f}j}}{L_{\text{f}i}} \tag{40}$$

Performing Laplace transformation on Eq. (38), we can obtain

$$\sum_{j=1}^{M} \sum_{i=1}^{N} \overline{q}_{fDi,j} \Delta L_{fDj} = \frac{1}{s}$$

$$\tag{41}$$

where $\overline{q}_{\text{fD}i,j}$ is the Laplace transformation of $q_{\text{fD}i,j}$.

Eq. (37b) actually represents M-1 equations, thus Eqs. (32), (37b) and (41) correspond to $M \times N + M$ equations. The total number of the unknowns is also $M \times N + M$, thus $\overline{q}_{\text{fD}i,j}(s)$ and $\overline{\xi}_{\text{wD}j0}(i=1, 2, 3, ..., N; j=1, 2, 3, ..., M)$ can be solved by Gaussian elimination method.

Since the wellbore pressure in different layers are the same, $\overline{\xi}_{\text{wDj0}}$ (j=1,2,3,...,M) is abbreviated as $\overline{\xi}_{\text{wD00}}$. According to van Everdingen and Hurst (1949), the effect of wellbore storage effect can be taken into account with the following equation

$$\overline{\xi}_{\text{WD0}} = \frac{s\overline{\xi}_{\text{WD00}}}{s + C_D s^2 \overline{\xi}_{\text{WD00}}}$$
(42)

where $\bar{\xi}_{wD0}$ is the Laplace transformation of ξ_{wD0} , and ξ_{wD0} is the zero-order analytical approximation of the dimensionless wellbore pseudo-pressure taking into account the effects of wellbore storage and skin factor; $\bar{\xi}_{wD00}$ is the Laplace transformation of ξ_{wD00} , and ξ_{wD00} is the zero-order analytical approximation of the dimensionless wellbore pseudo-pressure without wellbore storage and skin effect; C_D is the dimensionless wellbore storage coefficient.

With Stehfest numerical inversion method (Stehfest, 1970), the above analytical solution in the Laplace domain can be transformed into the real-time domain, and we can obtain the zero-order approximation of the wellbore pseudo-pressure as well as the production rate of different layers. Then with Eq. (9), the true wellbore pseudo-pressure can thus be obtained.

3.4. Conditions of applicability of the model

The proposed model, incorporating unequal initial formation pressure, limited fracture height and dual porosity medium, is proposed to interpret transient pressure behavior of vertically fractured well in multi-layered tight gas reservoirs. Although the model is proposed for naturally fractured reservoirs (i.e., dual-porosity medium), it can be applied to interpret transient pressure behavior of layered reservoir in which some layers of the reservoir can be homogeneous (by setting $\omega_j = 1$ and $\lambda_j = 0$ in the presented model). Under this condition, the expression of f(s) in Eq. (22) reduces to the following expression:

$$f(s) = \frac{\omega'_{j} \mu_{Rj} h_{Dj}^{2} L_{fDj}^{2}}{\gamma_{i}}$$
 (43)

Moreover, the model can also be applied to analyze the transient pressure responses of hydraulic fracture which fully penetrates the formation, by setting $h_{\rm wj}/h_j=1$ in the presented model. For hydraulic fractures fully penetrate the layer thickness, the basic zero-order line-sink solution in layer j, Eq. (25), reduces to:

$$\overline{\xi}_{sfDj0} = \frac{\overline{q_j(s)}}{q_{sc}\chi_j} \left[K_0(\alpha_{0,j}r_{Dj}) + \frac{K_1(\alpha_{0,j}r_{eDj})}{I_1(\alpha_{0,j}r_{eDj})} I_0(\alpha_{0,j}r_{Dj}) \right]$$
(44)

Moreover, the presented model and corresponding solution are derived for vertically fractured wells with a constant production rate. However, in practice the gas well may produce at variable production rates. With the superposition principle, the model can also be applied to analyze the transient pressure behavior of fractured wells with non-steady state production history, i.e., multirate production history. Assuming that the well produces at a sequence of rate $q_{\text{SC1}}, q_{\text{SC2}}, ..., q_{\text{SCn}}$, with respective starting times $t_1, t_2, ..., t_n$. Using the principle of superposition, we can calculate the transient pressure response of the fractured well by superposing the drawdown responses of constant-rate production, which can be expressed as follows:

$$\Delta \psi = \sum_{k=1}^{n} \left[q_{\text{sc}k} - q_{\text{sc}(k-1)} \right] \Delta \psi_{\text{unit}}(t - t_k)$$
 (45)

In addition, based on the superposition principle, the presented model can also be applied to interpret pressure responses collected during pressure build up process.

3.5. Possible extension of the model to gas—water two-phase flow

The object of this work is to present an analytical model to better understand the single-phase transient pressure behavior of a fractured well in multi-layer reservoirs. When the water saturation of the reservoir is below the irreducible water saturation, only single phase gas flows after well opening, which is valid at the early production stage of tight gas wells. However, in some cases, gas and water two-phase flow may occur due to the flowback after hydraulic fracturing. With the concept of pseudo-pressure of two-phase flow, the presented model can also be extended to investigate the transient pressure behavior of fractured wells in multi-layer gas reservoirs with gas—water two-phase flow.

The derivation of the two-phase flow model and corresponding solution strategy are briefly described here, providing an optional analytical approach to simulate wellbore pressure responses of tight gas reservoirs considering gas—water two-phase flow. More efforts will also be made in our future work.

Assuming that a continuous point-sink is located at point (x_{wj}, y_{wj}, z_{wj}) in layer j in a multi-layer gas reservoir, and single porosity medium is considered for simplicity. The gas production rate and water production rate of the point sink under standard condition are \hat{q}_{gscj} and \hat{q}_{wscj} . According to the derivation presented in Appendix B, we can obtain the following dimensionless model of the point-sink in layer j with gas—water two-phase flow.

$$\chi_{j} \left[\frac{\partial^{2} \psi_{sDj}}{\partial r_{Dj}^{2}} + \frac{1}{r_{Dj}} \left(\frac{\partial \psi_{sDj}}{\partial r_{Dj}} \right) + L_{fDj}^{2} \left(\frac{\partial^{2} \psi_{sDj}}{\partial z_{Dj}^{2}} \right) \right] = \omega_{j}' h_{Dj}^{2} L_{fDj}^{2} \mu_{Rj} \frac{\partial \psi_{sDj}}{\partial t_{D}}$$

$$(46)$$

$$\psi_{sDj}(r_{Dj}, z_{Dj}, t_D)\big|_{t_D=0} = 0$$
 (47)

$$\left.\frac{\partial \psi_{sDj}\big(r_{Dj},z_{Dj},t_{D}\big)}{\partial r_{Dj}}\right|_{r_{Dj}=r_{eDj}}=0 \ \ (impermeable\ lateral\ boundary) \end{matrix}$$

$$\left.\frac{\partial \psi_{sDj}(r_{Dj},z_{Dj},t_D)}{\partial z_{Dj}}\right|_{z_{Dj}=0}=0 \ \ (impermeable \ upper \ boundary)$$

$$\left. \frac{\partial \psi_{\text{SD}j} \left(r_{\text{D}j}, z_{\text{D}j}, t_{\text{D}} \right)}{\partial z_{\text{D}j}} \right|_{z_{\text{D}j} = h_{\text{D}j}} = 0 \ \ (\text{impermeable lower boundary})$$
(50)

$$\lim_{\varepsilon_{\rm Dj}\to 0} \int_{z_{\rm wDj}-\varepsilon_{\rm Dj}/2}^{z_{\rm wDj}+\varepsilon_{\rm Dj}/2} \left[\lim_{\sigma_{\rm Dj}\to 0} \chi_j \left(r_{\rm Dj} \frac{\partial \psi_{\rm sDj}}{\partial r_{\rm Dj}} \right)_{r_{\rm Dj}=\sigma_{\rm Dj}} \right] dz_{\rm Dj} = -\widehat{q}_{\rm Dj}(t_{\rm D}) \quad (51)$$

The definitions of relevant dimensionless parameters are as follows:

$$\psi_{\text{sD}j} = \frac{2\pi (k_{\text{h}}h)_{\text{t}}}{\left(\rho_{\text{gsc}}q_{\text{gsc}} + \rho_{\text{wsc}}q_{\text{wsc}}\right)} (\psi_{\text{l}j} - \psi_{j}) \tag{52a}$$

$$t_{\rm D} = \left(\frac{\rho_{\rm g1} k_{\rm rg1}}{\mu_{\rm g1}} + \frac{\rho_{\rm w1} k_{\rm rw1}}{\mu_{\rm w1}}\right) \cdot \frac{(k_{\rm h} h)_{\rm t}}{\left(\phi_{\it j} h_{\it j} C_{\it j}\right)_{\rm t} r_{\rm w}^2} t \tag{52b}$$

$$\mu_{Rj} = \frac{\frac{\rho_{g1}k_{rg1}}{\mu_{g1}} + \frac{\rho_{w1}k_{rw1}}{\mu_{w1}}}{\frac{\rho_{gj}k_{rgj}}{\mu_{wj}} + \frac{\rho_{wj}k_{rwj}}{\mu_{wi}}}$$
(52c)

$$\widehat{q}_{Dj}(t_D) = \frac{\rho_{gsc}\widehat{q}_{gscj} + \rho_{wsc}\widehat{q}_{wscj}}{\rho_{gsc}q_{gsc} + \rho_{wsc}q_{wsc}}$$
(52d)

$$\omega_{j}' = \frac{\phi_{j} h_{j} C_{j}}{\left(\phi_{j} h_{j} C_{j}\right)_{t}} \tag{52e}$$

The definitions of other dimensionless parameters are the same as those presented in Table 1.

The model expressed by Eqs. (1)–(8) is referred to as single-phase model, and the model expressed by Eqs. (46)–(51) is referred to as two-phase model. Comparing these two models, we can find that they share similar expressions. By setting $\omega_j=1$ and $\lambda_j=0$, the dimensionless form of single-phase model is exactly the same as the two-phase model, indicating that the solution strategy presented in Sections 3.1 to 3.3 can be directly adopted to obtain analytical solutions of the gas—water two-phase flow model. Similarly, the influence of stress sensitivity can also be incorporated by applying the Pedrosa's transformation and the perturbation method.

4. Model validation

To the best of our knowledge, semi-analytical solutions for fractured vertical wells incorporating different fracture penetration ratio, dual porosity and unequal initial reservoir pressures in multilayer reservoirs have not been reported in the literature. Therefore, two simplified cases are used to verify the reliability of the proposed model in this work. The calculated results of the proposed model were compared with those obtained by Saphir, a commercial software designed for transient pressure data analysis and interpretation. The commercial software offers limited height fracture option for multi-layer reservoirs. However, it can only handle single porosity reservoirs with infinitely large outer boundary condition.

To compare the results calculated with the proposed model with the results obtained from the commercial software, the proposed model is simplified into single porosity medium by setting $\omega_j=1$, and the item $\frac{K_1(\alpha_{n,j}r_{\text{ED}j})}{I_1(\alpha_{n,j}r_{\text{ED}j})}I_0(\alpha_{n,j}r_{\text{D}j})$ in Eq. (21) is set as zero to model the infinitely large outer boundary case.

Two sets relevant parameters of well, fluid, hydraulic fracture, and reservoir are given in Table 2. Fig. 3 shows the comparisons of the transient pressure responses calculated by the proposed model in this paper with results calculated by the commercial software. It can be seen that for the two cases, the calculated results obtained by the proposed model match excellently with the results given by the commercial software, which verifies the accuracy and reliability of the proposed mathematical model and corresponding solutions.

5. Results and discussion

Based on the above presented model, a synthetic case under the condition of constant gas production rate is calculated to identify the characteristic flowing regimes and to discuss the influences of relevant factors on transient pressure dynamics. The basic parameters of well, fluid, hydraulic fractures, and reservoir for the synthetic case are presented in Table 3, other parameters are same as those presented in Table 2.

 Table 2

 Detailed input parameters used in the model validation cases.

| Parameter | Value | | | | | |
|---|-------------|--------------|-------------|-------------|--------------|-------------|
| | Case 1 | | | Case 2 | | |
| | First layer | Second layer | Third layer | First layer | Second layer | Third layer |
| Half-length of hydraulic fracture, m | 50 | 70 | 60 | 65 | 85 | 70 |
| Formation thickness, m | 18 | 10 | 14 | 8 | 13 | 11 |
| Formation horizontal permeability, mD | 0.6 | 0.4 | 0.2 | 0.5 | 0.7 | 0.3 |
| Permeability ratio k_{vi}/k_{hi} | 0.76 | 0.78 | 0.77 | 0.74 | 0.76 | 0.72 |
| Formation porosity, % | 7 | 9 | 8 | 8.3 | 9.2 | 7.8 |
| The ratio of the hydraulic fracture height to the formation thickness | 0.65 | 0.63 | 0.64 | 0.66 | 0.64 | 0.68 |
| Initial formation pressure, MPa | 22.6 | 22.6 | 22.6 | 31.7 | 31.7 | 31.7 |
| Initial formation temperature, °C | 49 | 49 | 49 | 56 | 56 | 56 |
| Total compressibility, MPa ⁻¹ | 0.037 | 0.037 | 0.037 | 0.021 | 0.021 | 0.021 |
| Initial gas viscosity, mPa·s | 0.021 | 0.021 | 0.021 | 0.025 | 0.025 | 0.025 |
| Wellbore radius, m | 0.1 | | | 0.1 | | |
| Production rate of gas well, m ³ /d | 80000 | | | 60000 | | |
| Wellbore storage coefficient, m ³ /MPa | 0.117 | | | 0.152 | | |
| Skin factor | 0.1 | | | 0.13 | | |

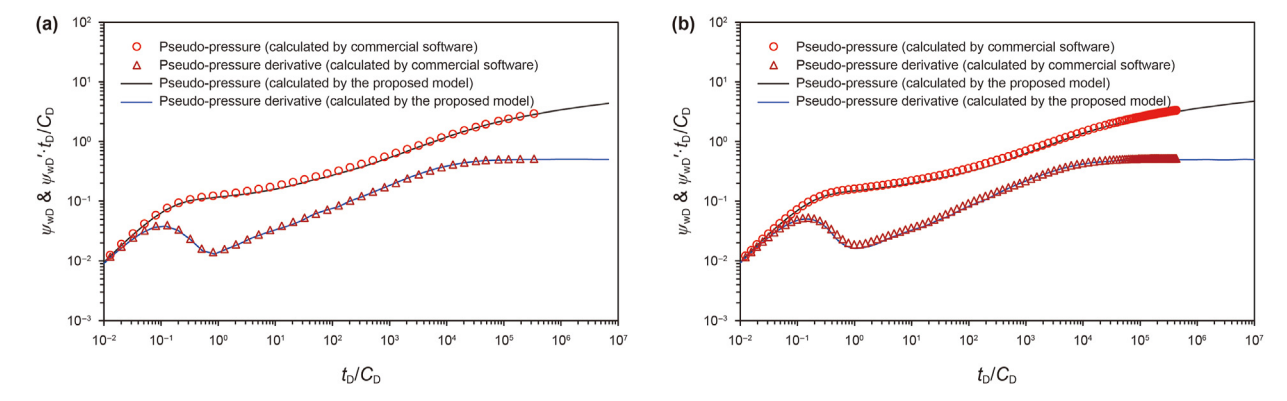


Fig. 3. Comparisons of transient pressure responses calculated by the proposed model in this paper with results obtained by a commercial software. (a) Case 1; (b) case 2.

Table 3The physical properties of well, fluid, hydraulic fractures, and reservoir in the synthetic case.

| Parameter | Value | | | |
|---|-------------------------------|-------------------------------|-------------------------------|--|
| | First layer | Second layer | Third layer | |
| The ratio of the hydraulic fracture height to the formation thickness | 0.65 for dual-porosity case; | 0.63 for dual-porosity case; | 0.64 for dual-porosity case; | |
| | 0.52 for single-porosity case | 0.53 for single-porosity case | 0.51 for single-porosity case | |
| Inter-porosity flowing coefficient | 1.4×10^{-6} | 1.2×10^{-6} | 1.1×10^{-6} | |
| Storativity ratio of each layer | 0.11 | 0.12 | 0.13 | |
| Formation radius, m | 760 | 780 | 740 | |
| Initial formation pressure, MPa | 22.4 | 22.6 | 22.8 | |
| Total compressibility, MPa ⁻¹ | 0.037 | 0.037 | 0.037 | |
| Initial gas viscosity, mPa·s | 0.021 | 0.021 | 0.021 | |

5.1. Flowing regimes

Fig. 4 presents the dimensionless type curves of a fractured vertical well in a dual-porosity reservoir with multi-layers. The initial reservoir pressures, half-length of the hydraulic fracture, and the radius of the outer boundary are unequal for different layers. The upper red line and the lower blue line represent the wellbore pseudo-pressure and pressure derivative, respectively. According to Fig. 4, the transient pressure behavior can be divided into 7 characteristic flowing regimes.

(1) Wellbore storage period. During the starting-up process of the well, the initial surface production rate of the well is

- nearly totally contributed by the compressibility of the fluid stored in the wellbore, resulting in a difference between the sandface flow rate and the wellhead flow rate. During this flowing period, both the pressure and the pressure derivative curves exist a unit-slope straight line. The duration of this flowing period is mainly controlled by the value of the wellbore storage coefficient.
- (2) The transitional flowing period. During this period, the sandface flow rate gradually increases until it becomes equal to the wellhead flow rate. The flowing period is characterized by a "hump" in the pressure derivative curve, and the duration of this flowing period is up to the combination of the wellbore storage coefficient and the skin factor.

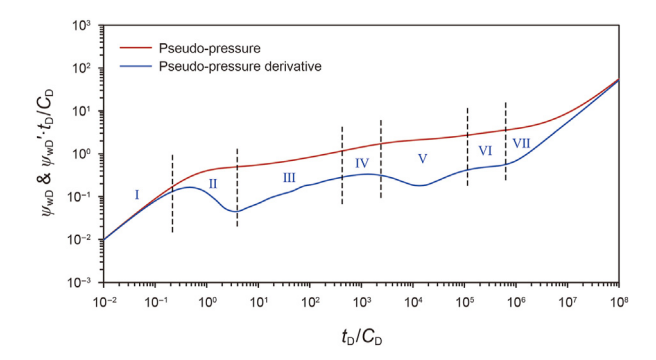


Fig. 4. Transient pressure behavior of a fractured vertical well in a dual-porosity threelayer reservoir.

- (3) Reservoir linear flow period. Linear gas flowing perpendicular to the hydraulic fracture over a limited vertical interval (the fracture height) occurs in each layer of the reservoir (Fig. 5(a)), and a straight line with a slope of "1/2" appears in the pressure derivative curve. The duration of the linear flow period depends on the parameters of the hydraulic fracture and layer properties.
- (4) The vertical pseudo-radial flow in the natural fracture system. As the well continues to produce, the pressure wave propagates further into the formation. When the hydraulic fracture doesn't fully penetrate the whole formation layer, approximate radial flow (i.e., pseudo-radial flow) can be observed around the hydraulic fractures (Fig. 5(b)). A horizontal line can be observed in the pressure derivative curve at this stage. The duration of this flow regime depends on the ratio of the fracture height to the formation thickness. As the height of the hydraulic fracture gradually approaches the formation thickness, this flowing period may not be observed in the type curves.
- (5) Inter-porosity flow between natural fracture and matrix system. The pressure of natural fracture system decreases due to the production of natural gas, resulting in pressure difference between natural fracture and matrix system. Therefore, natural gas stored in the matrix system flows into the natural fracture system driven by the pressure difference, providing energy for the natural fracture system. As a result, the pressure depletion rate of natural fracture system and the bottomhole pressure becomes smaller, which is reflected by a characteristic "dip" in the pressure derivative curve. The appearance time and the shape of the "dip" are mainly affected by the storativity ratio and the inter-porosity coefficient of the dual porosity reservoir.
- (6) The late-time pseudo-radial flow in the natural fracture and matrix systems. With the continuous gas flowing from matrix to natural fractures, the pressure difference between the natural fracture and matrix system decreases until it reaches zero. Then the pseudo-radial flow of the total system appears, and gas flows radially toward the hydraulic fracture in each individual layer (Fig. 5(c)). This flowing period is characterized by a flat line in the pressure derivative curve, and the value of the pressure derivative curve during this flowing period is "0.5".
- (7) Boundary-dominated flowing period. As the production time elapses, the pressure wave eventually reaches the impermeable boundary of the reservoir, and the well enters the boundary-dominated flowing period. During this period, both the dimensionless pressure curve and the pressure derivative curve exhibit as a unit-slope straight line. The occurrence time of the late-time boundary-dominated

flowing period mainly depends on the value of radius of the reservoir boundary.

It should be mentioned that due to the influence of interporosity flowing, the characteristics of some flowing periods may be covered and cannot be observed in the dimensionless type curves. Fig. 6 shows the dimensionless type curves of a fractured vertical well in a single-porosity reservoir with multi-layers. The corresponding transient pressure behavior can also be divided into 7 characteristic flowing regimes, in which the characteristics of the flowing periods (1) to (3) and periods (5) to (7) are similar to Fig. 4. In Fig. 6, after the reservoir linear flow period (i.e., period 3), another straight line with a slope of "1/2" can be observed in the pressure derivative curve, which is a reflection of the second-linear flow period. During this period, linear gas flowing occurs over the whole formation thickness in each layer of the reservoir (Fig. 5(d)).

5.2. Sensitivity analysis

Fig. 7 shows the influence of unequal initial formation pressures on the dimensionless transient pressure behavior of a fractured vertical well in a dual-porosity reservoir with multi-layers. In Fig. 7, the upper solid lines and lower lines with dots represent the dimensionless pressure and pressure derivative curves, respectively. In the synthetic case, the initial pressure of layer 3 is the highest and is kept unchanged during the calculation. It can be observed that unequal initial formation pressure mainly affects the early-time transient pressure behavior of the fractured vertical well in the dual-porosity three-layer reservoir. The pressure derivative curve during the transitional flowing period is higher when the dimensionless initial pressures increase. This is because $\psi_{\text{ID}i}$ is defined based on the maximum initial pressure of the multi-layer reservoir (as shown in Table 1), $\psi_{\text{ID}j} = 0$ denotes that all three layers in the reservoir have the same initial pressures, and a positive value of $\psi_{\text{ID}i}$ denotes larger initial pressure difference between different layers. With the same total production rate and the same initial pressure of layer 3, as the dimensionless initial pressures of layer 1 and layer 2 increase, the pressure drops caused by the production in the layers with lower initial pressures (layer 1 and layer 2 in the case) are larger, which is reflected by higher location of the pressure derivative curve.

The proposed model can consider the case of limited fracture height in dual-porosity multi-layer gas reservoirs. Fig. 8 shows the effect of the hydraulic fracture height on the transient pressure behavior of a fractured vertical well in a dual-porosity three-layer reservoir. It is found that the limited fracture height mainly has effect on the transient pressure behavior during the reservoir linear flow period. As the ratio of the hydraulic fracture height to the layer thickness increases, the contact area between the infinite-conductivity hydraulic fracture and the reservoir increases, leading to lower pressure drop during production.

Fig. 9 shows the influence of the hydraulic fracture half-length on the transient pressure behavior of a fractured vertical well in a dual-porosity three-layer reservoir. As shown in Fig. 9, the variation of fracture length has obvious influence on the transient pressure behavior during the transitional flowing period, the reservoir linear flow period, and the vertical pseudo-radial flowing period. With the increase in fracture half-length, the pressure curve and pressure derivative curve during the above periods drop down, indicating smaller pressure drop. When the value of the fracture half-length increases to a certain value, the vertical pseudo-radial flowing period may not be observed in the transient pressure and pressure derivative curves.

Figs. 10 and 11 show the influence of the parameters related to dual-porosity medium. It is found that the variations of the

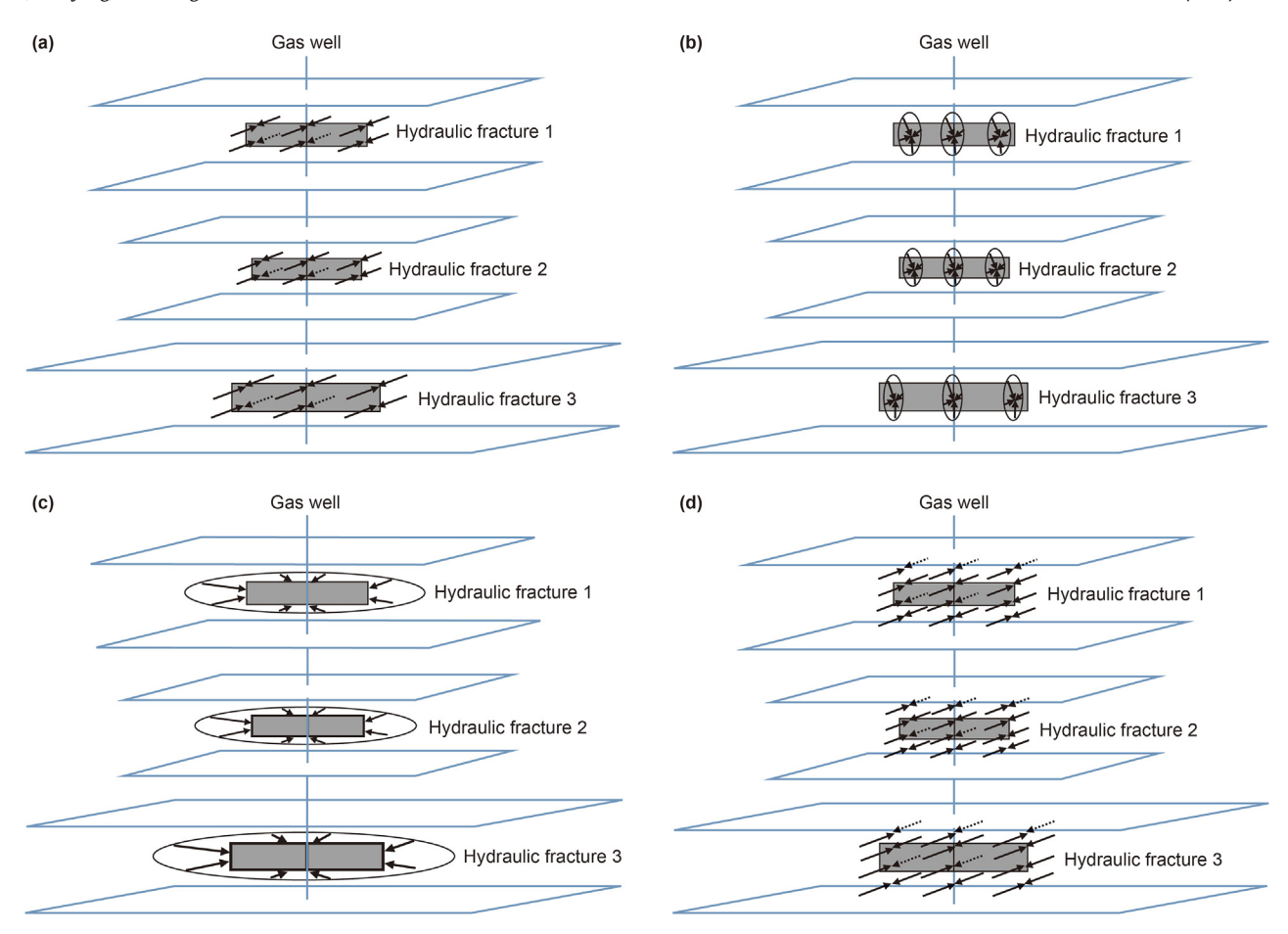


Fig. 5. Schematic of the characteristic flowing periods. (a) The reservoir linear flow; (b) the first vertical pseudo-radial flow; (c) the late-time pseudo-radial flow; (d) the second linear flow.

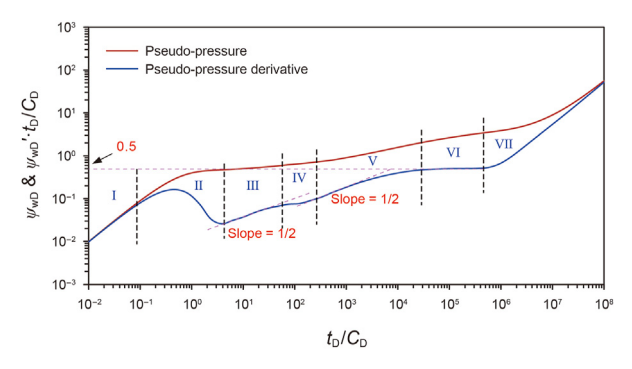


Fig. 6. Transient pressure behavior of a fractured vertical well in a single-porosity three-layer reservoir.

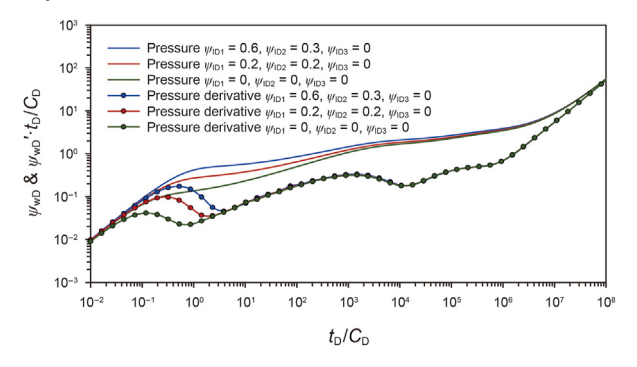


Fig. 7. Transient pressure behavior of a fractured vertical well in a dual-porosity three-layer reservoir with unequal initial pressures.

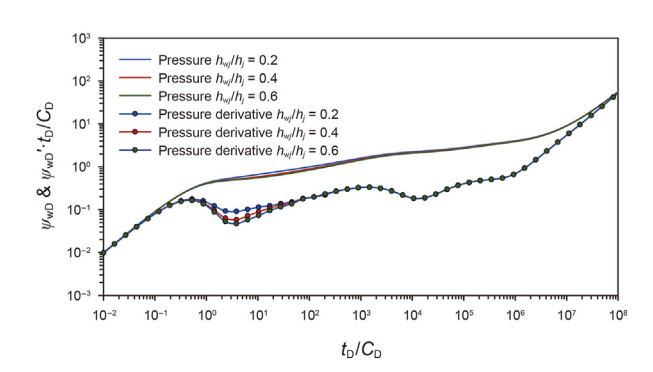


Fig. 8. Effect of limited fracture height on the transient pressure behavior of a fractured vertical well in a dual-porosity three-layer reservoir.

storativity ratio and inter-porosity coefficient have primary effect on the transient pressure behavior during inter-porosity flow period. With the decrease in the storativity ratio, the "dip" in the pressure derivative curve becomes more obvious. For larger interporosity coefficient, the inter-porosity flowing between natural fracture system and matrix occurs earlier, and the appearance time of the "dip" in the pressure derivative curve is also earlier. In addition, the variation of the storativity ratio also affects the pressure behavior during the reservoir linear flow and the vertical pseudo-radial flow periods. It can be seen from Fig. 10 that smaller value of the storativity ratio leads to higher position of the pressure and pressure derivative curves during reservoir linear flow period.

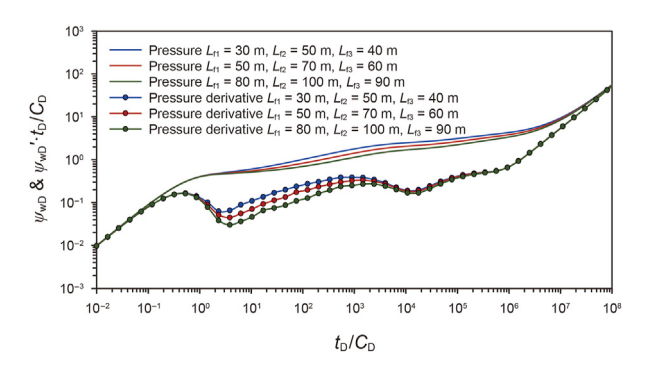


Fig. 9. Effect of fracture half-length on the transient pressure behavior of a fractured vertical well in a dual-porosity three-layer reservoir.

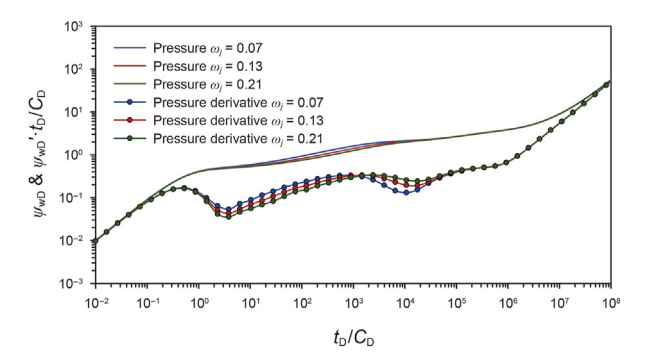


Fig. 10. Effect of storativity ratio on the transient pressure behavior of a fractured vertical well in a dual-porosity three-layer reservoir.

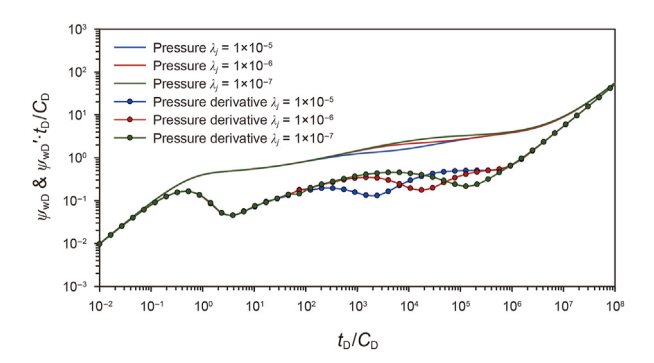


Fig. 11. Effect of inter-porosity flowing coefficient on the transient pressure behavior of a fractured vertical well in a dual-porosity three-layer reservoir.

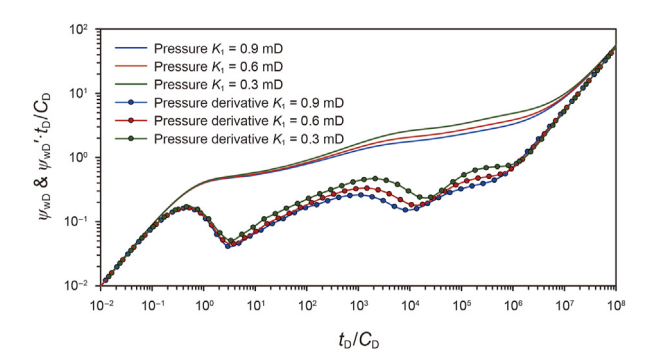


Fig. 12. Effect of formation permeability on the transient pressure behavior of a fractured vertical well in a dual-porosity three-layer reservoir.

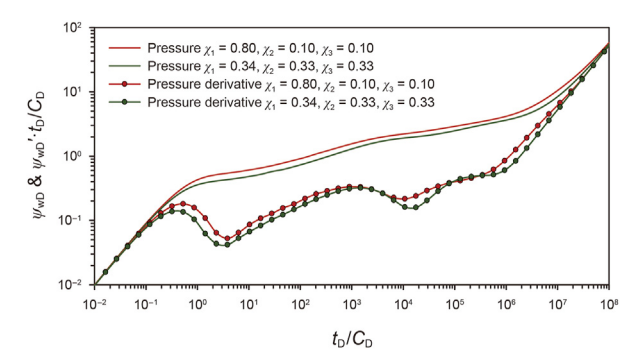


Fig. 13. Effect of formation coefficient ratio on the transient pressure behavior of a fractured vertical well in a dual-porosity three-layer reservoir.

Fig. 12 shows the comparison of transient pressure responses for different values of formation permeability of layer 1. All other parameters, including the parameters of hydraulic fracture, parameters of dual-porosity medium, stay the same. Since the dimensionless pseudo-pressure and dimensionless time are defined based on the summation of the permeability-thickness product of multiple layers $((k_{fh}h)_t)$, while the variation of permeability of layer 1 will inevitably affect the specific values of dimensionless pseudo-pressure and dimensionless time. In order to compare the pseudo-pressure responses for different values of formation permeability, all the dimensionless pseudo-pressures and dimensionless time are evaluated based on the base case presented in Table 2 (i.e., $K_1 = 0.6$ mD). As the formation permeability increases, the pressure wave spreads faster in the reservoir. The larger the formation permeability is, the earlier the flow regimes III to VII appear. On the other hand, with the same constant production rate, the larger the permeability is, the smaller the pressure drop, corresponding to lower position of dimensionless pressure and pressure derivative curves.

Fig. 13 compares the transient pressure responses for two cases with different values of formation coefficient ratio, χ_j . In the first case the formation coefficient ratios of all three layers are approximately the same ($\chi_1=0.34,\,\chi_2=0.33,\,\chi_3=0.33$), which is referred to as the uniform formation coefficient ratio case. While in the second case, the formation coefficient ratios of the three layers are quite different ($\chi_1=0.80,\,\chi_2=0.10,\,\chi_3=0.10$), which is referred to as the non-uniform formation coefficient ratio case. It should be mentioned that the summation of the permeability-thickness product of multiple layers ($\left(k_{\rm fh}h\right)_{\rm t}$) is kept constant in the two cases. We can observe that the formation coefficient ratio, χ_j , affects almost all the flow regimes except for the wellbore storage period.

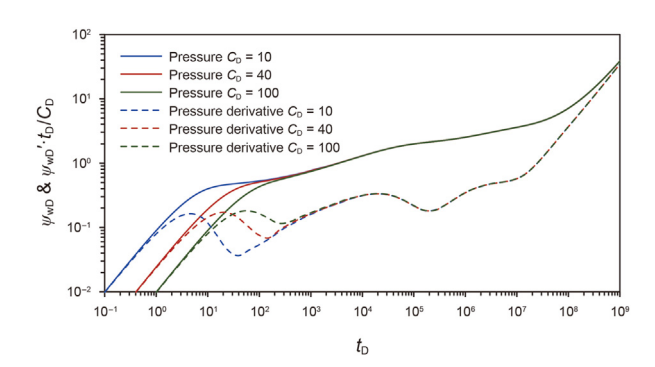


Fig. 14. Effect of wellbore storage on the transient pressure behavior of a fractured vertical well in a dual-porosity three-layer reservoir.

The larger the difference between the χ_j of different layers, the higher the dimensionless pressure and pressure derivative curves. Compared with the uniform formation coefficient ratio case, the inter-porosity flow and boundary-dominated flow periods appear earlier for the non-uniform case. This is because in the non-uniform case, the formation coefficient ratio of layer 1 is obviously larger than other layers, indicating obviously larger permeability of layer 1. The propagation of pressure wave in the layer 1 is faster than that in the uniform formation coefficient ratio case, resulting in earlier reflection of inter-porosity flow and boundary-dominate flow periods in the dimensionless pressure derivative curves.

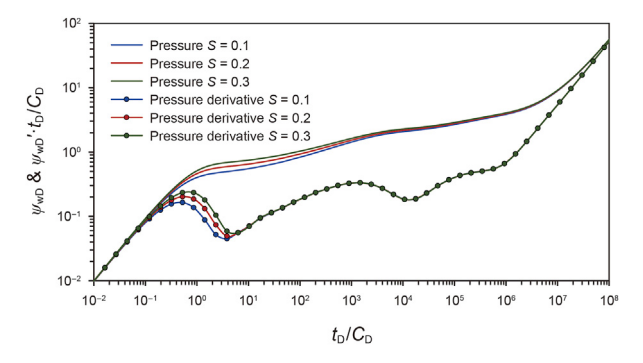


Fig. 15. Effect of skin factor on the transient pressure behavior of a fractured vertical well in a dual-porosity three-layer reservoir.

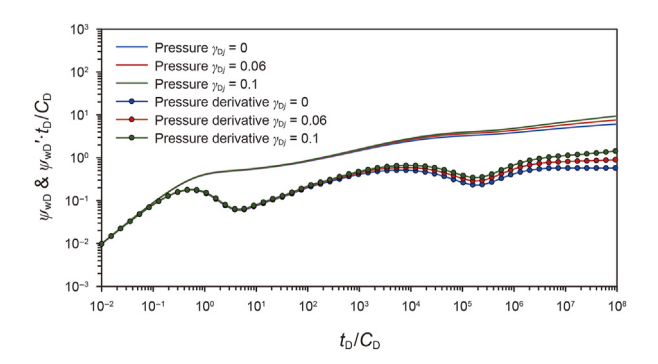


Fig. 16. Effect of stress sensitivity on the transient pressure behavior of a fractured vertical well in a dual-porosity three-layer reservoir.

Figs. 14 and 15 show the dimensionless pressure and pressure derivative curves with different wellbore storage and skin factors, separately. Results show that the wellbore storage has significant influence on early-time flow regimes including wellbore storage period, transitional flowing period, and reservoir linear flow period. When the value of wellbore storage coefficient increases to a certain extent, early time transient pressure responses may be masked by wellbore storage. On the other hand, the value of skin factor mainly affects the amplitude of the hump in the pressure derivative curve during the transitional flowing period, and a larger skin factor will always correspond to a larger hump.

Fig. 16 shows the influence of stress sensitivity modulus on transient pressure responses of a fractured vertical well in a dualporosity three-layered gas reservoir. As can be seen, the stress sensitivity mainly affects the intermediate to late time transient pressure responses. During early production stage, no significant difference can be observed in the transient pressure compared with no stress sensitivity case. This is because the pressure drop at early production stage is relatively small, the change in the pore-throat structure and reduction of permeability is not obvious. As production continues, the pressure drop in the gas reservoir increases, and the decrease in permeability caused by stress sensitivity becomes more obvious. Gas flowing in the formation needs to overcome larger flowing resistance, leading to an upward tendency of dimensionless pseudo-pressure and derivative curves. With the increase in the stress sensitivity modulus, the upward of dimensionless pseudo-pressure and derivative curves becomes more

In the proposed model, the production rate of the commingled production gas well is set as constant; however, the gas volume produced from different layers is different, and it varies with production time. In order to analyze the characteristics of production contribution by different layers, another synthetic case is designed to obtain the production performance of each layer under the condition of constant total production rate. The basic parameters of well, fluid, hydraulic fractures, and reservoir adopted in the basic synthetic case are presented in Table 4.

Fig. 17 presents the production rate contribution of individual layer in a three-layer gas reservoir. The total production rate of the fractured well is set as constant. Except for formation permeability, other parameters of different layers are all the same. It can be observed that the gas output of the well at the initial stage is mainly contributed by the high-permeability layer, i.e., layer 1 in Fig. 17. With the increasing production time, the production contribution

 Table 4

 The physical properties of well, fluid, hydraulic fractures, and reservoir in the synthetic case for production contribution analysis.

| Parameter | Value | | | |
|---|----------------------|----------------------|----------------------|--|
| | First layer | Second layer | Third layer | |
| Half-length of hydraulic fracture, m | 50 | 50 | 50 | |
| Formation thickness, m | 14 | 14 | 14 | |
| Formation horizontal permeability, mD | 0.4 | 0.4 | 0.4 | |
| Permeability ratio k_{fvi}/k_{fhi} | 0.75 | 0.75 | 0.75 | |
| Total formation porosity, % | 11 | 11 | 11 | |
| Formation radius, m | 760 | 760 | 760 | |
| The ratio of the hydraulic fracture height to the formation thickness | 0.65 | 0.65 | 0.65 | |
| Inter-porosity flowing coefficient | 1.0×10^{-6} | 1.0×10^{-6} | 1.0×10^{-6} | |
| Storativity ratio | 0.13 | 0.13 | 0.13 | |
| Initial formation pressure, MPa | 22.8 | 22.8 | 22.8 | |
| Initial formation temperature, °C | 49 | 49 | 49 | |
| Total compressibility, MPa ⁻¹ | 0.037 | 0.037 | 0.037 | |
| Initial gas viscosity, mPa·s | 0.021 | 0.021 | 0.021 | |
| Wellbore radius, m | 0.1 | | | |
| Production rate of gas well, m ³ /d | 80000 | | | |
| Wellbore storage coefficient, m ³ /MPa | 0.117 | | | |
| Skin factor | 0.1 | | | |

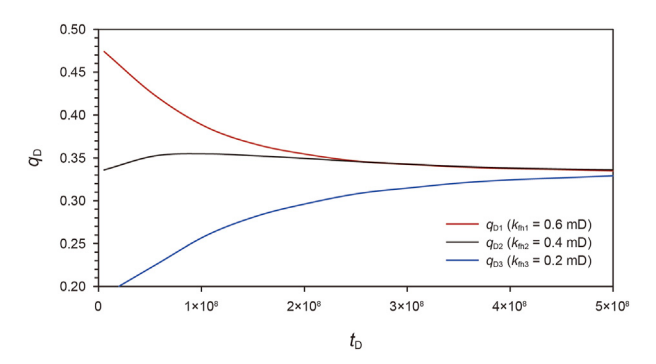


Fig. 17. Effect of permeability difference on the production rate contribution of a fractured vertical well in a dual-porosity three-layer reservoir.

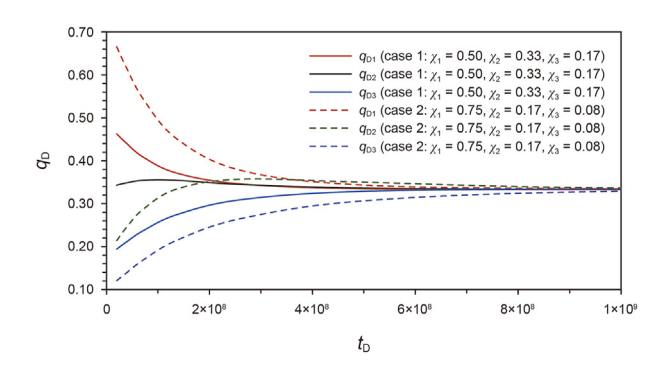


Fig. 18. Effect of formation coefficient ratio on the production rate contribution of a fractured vertical well in a dual-porosity three-layer reservoir.

of the high-permeability layer gradually decreases, while the production contributions of the medium- and low-permeability layers gradually increase. This is because the cumulative gas volume produced from the high-permeability layer is larger compared with the other two layers, thus the pressure depletion in the high-permeability layer (layer 1) is also more obvious. While the formation pressure of the other low-permeability layers is relatively higher, the gas production from the low-permeability layers gradually increases at intermediate and late stages, and the difference between production contributions of high-permeability and low-permeability layers gradually diminishes.

Fig. 18 shows the comparison of production rate contributions of individual layer in a three-layer gas reservoir with different formation coefficient ratios. In the two cases presented in Fig. 18, the formation coefficient ratio of layer 1 (i.e., χ_1) is the largest, while the formation coefficient ratio of layer 3 (i.e., χ_3) is the smallest among the three layers. Similar to Fig. 17, gas production of different layers varies at different production stages. At the initial stage, the gas production mainly results from the high-permeability layer (layer 1). As the well continues to produce, the contribution of layers with relatively smaller permeabilities (layer 2 and layer 3) gradually increases at the intermediate and late stages as the energy of highpermeability layer has been consumed significantly. Comparing the production rate contributions of the two cases in Fig. 18, the larger the difference between layer properties, the more obvious the difference between production contributions from different layers. The difference between χ_1 and χ_3 in case 2 is larger, causing the production contribution of layer 1 at the early stage in case 2 is also obviously larger than that in case 1.

Fig. 19 shows the production contributions of individual layer for a commingle production well in a dual-porosity three-layer reservoir, in which the length of the hydraulic fracture in each layer

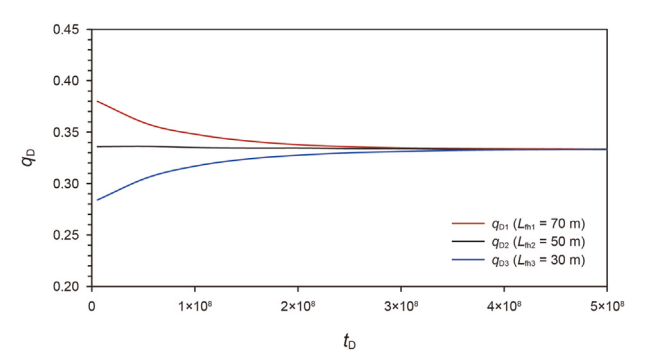


Fig. 19. Effect of fracture half-length on the production rate contribution of a fractured vertical well in a dual-porosity three-layer reservoir.

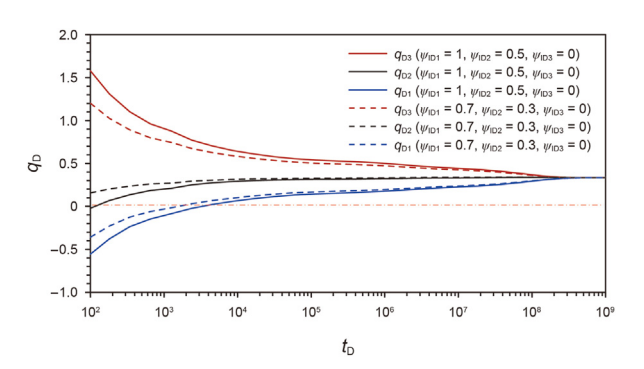


Fig. 20. Effect of unequal initial pressures on the production rate contribution of a fractured vertical well in a dual-porosity three-layer reservoir.

is different. It can be seen that the fracture half-length has primary influence on production contribution at initial stage, while it has little effect on the production contribution during intermediate and late stages. During the initial production period, the layer with larger fracture length produces more gas. As the pressure wave gradually propagates in the formation, the influence of fracture half-length gradually decreases, and the production contribution difference also gradually decreases with increasing production time.

Fig. 20 shows the production contribution of each layer in a dual-porosity three-layer reservoir under the condition of constant total production rate. In order to observe the production contribution of different layers at the initial period more clearly, the xaxis in Fig. 20 is shown in the logarithmic coordinate. Two cases are presented in Fig. 20, and the solid lines correspond to the production rates of multiple layers in case 1, in which the initial pressures of the three layers are $\psi_{\text{ID1}} = 1$, $\psi_{\text{ID2}} = 0.5$, and $\psi_{\text{ID3}} = 0$. The dashed lines correspond to the production rates of multiple layers in case 2, in which the initial pressures of the three layers are $\psi_{\text{ID1}}=0.7$, $\psi_{\text{ID2}}=0.3$, and $\psi_{\text{ID3}}=0$. It can be observed that the production rate of the fractured well is mainly contributed from the high-pressure layer at the initial period. It should also be addressed that due to the unequal initial pressures, the bottomhole flowing pressure may be higher than the formation pressure of the lowpressure layer at the initial stage. Thus, the gas will flow from the high-pressure layer to the low-pressure layer (i.e., gas backflow phenomenon), and the initial gas production rate of the lowpressure layer is negative. The gas backflow phenomenon will cause interlayer interference and prohibit the efficient recovery of the low-pressure layer. As the production time increases, the bottomhole flowing pressure decreases gradually. When the bottomhole flowing pressure is lower than the formation pressure of the

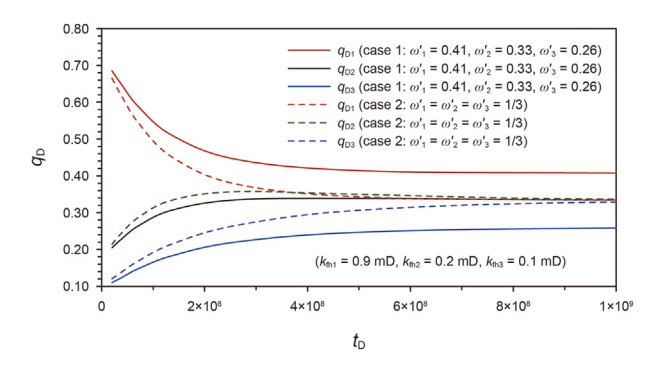


Fig. 21. Effect of storativity ratio of multiple layers on the production rate contribution of a fractured vertical well in a dual-porosity three-layer reservoir.

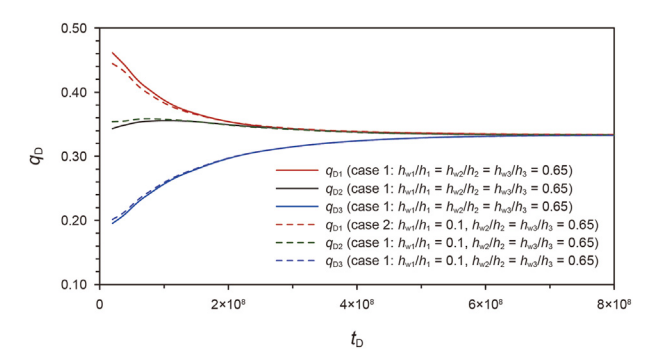


Fig. 22. Effect of limited fracture height on the production rate contribution of a fractured vertical well in a dual-porosity three-layer reservoir.

low-pressure layer, the gas backflow in the low-pressure stops, and the contribution of the low-pressure layer gradually increases. Larger difference between the unequal initial formation pressures will cause longer duration of the backflow and larger backflow volume. Compared with case 2 in Fig. 20, the difference between layer 1 and layer 3 in case 1 is larger, and the gas backflow volume in case 1 is also larger. At the intermediate and late stage, the pressure of high-pressure layer (layer 1 in Fig. 20) gradually declines due to gas production, while the pressures of the low-pressure layers (layer 2 and layer 3) remain at a relatively high level because the productions from these two layers at initial stage are much smaller. As a result, the production of the high-pressure layer gradually decreases due to insufficient energy, while the contribution of the low-pressure layers (layer 2 and layer 3) gradually increases.

Fig. 21 shows the effect of storativity ratio of multiple layers, ω'_j , on production contribution of each layer in a dual-porosity three-layer reservoir. Two cases are presented in Fig. 21, and the vertical permeability distribution of different layers are the same in the two cases. It is obvious that the ω'_j has significant influence on the production contribution of individual layer in a multi-layer system. At early stage of production, the gas contribution of different layers is mainly dependent on the product of layer permeability and layer thickness. Because the vertical distributions of layer permeability and layer thickness are same in the two cases, the gas production contribution of different layers at initial stage is quite similar. The storativity ratio, which reflects the relative storage capacity of different layers, has primary effect on production rate contribution after initial stage. The larger the storativity ratio of individual layer (for example, layer 1 in case 1), the larger the production

contribution of the layer during the intermediate and late stages.

Fig. 22 shows the influence of fracture height on the production contribution of each layer in a dual-porosity three-layer reservoir. In the two cases presented in Fig. 22, the fracture penetration ratios of layer 1 are different, while other parameters, including the fracture penetration ratios of other two layers, the storativity ratio and the formation coefficient ratio, are kept unchanged. It can be seen that the fracture height has a primary influence on the early-time production behavior. Because layer 1 is the high-permeability layer, the production contribution of layer 1 at initial stage is obviously larger compared with the other two layers. With the decrease in the fracture penetration ratio of layer 1, the production contribution of layer 1 also decreases. As production continues, the influence of fracture penetration on production contribution gradually decreases, which is consistent with the phenomena observed in Fig. 8.

6. Field case

In this section, two case studies are performed to show the practicality of the proposed model. Fig. 23 shows the procedures to obtain reservoir and fracture parameters with the proposed model. The basic parameters of well, individual layer, natural gas and hydraulic fracture are obtained from drilling data, well logging interpretation results, laboratory experiments, and fracture propagation modeling results or micro-seismic monitoring. Based on these basic parameters, theoretical and measured pseudo-pressure and pressure derivative curves can thus be calculated. Based on the characteristics of measured log-log curves, the type curve fitting procedure is conducted to obtain an acceptable match between theoretical and measured curves. During this process, the production logging data, which provides layer contribution, is adopted to determine the formation coefficient ratio. For well testing problems of multi-layer reservoirs, production logging data can help reduce the non-uniqueness of well testing interpretation, and is necessary for determination of physical parameters of individual layer.

6.1. Case study 1

The proposed model is applied to analyze the transient pressure data collected from a gas well (well A) to demonstrate its applicability. Well A is a two-layer commingled production gas well, which is located in the Sichuan Basin in China. The reservoir temperature is 82 °C, and the specific gravity of the produced natural gas is 0.601. The wellbore radius is 0.08 m. Before putting into production, each layer produced by well A was stimulated by hydraulic fracturing, separately. The total production time of well A is about 5000 h before the buildup test, and the total duration of the buildup test is 407.3 h.

Because of the lack of separate layer testing data, the transient bottomhole pressure data collected during the buildup testing was analyzed by our proposed model based on the workflow shown in Fig. 23. The pressure and pressure derivative matching of well A is shown in Fig. 24(a), and the corresponding interpretation results are shown in Table 5. It can be seen that the theoretical pressure and pressure derivatives calculated by the proposed model fit perfectly with the measured data. The pressure history matching results of well A are shown in Fig. 24(b), which indicates the interpretation results are reasonable and acceptable.

As mentioned earlier, the production logging data is crucial to accurate determination of parameters of individual layers. Because of the lack of production logging data for well A, the layer contribution data provided by another well in the same block was used to

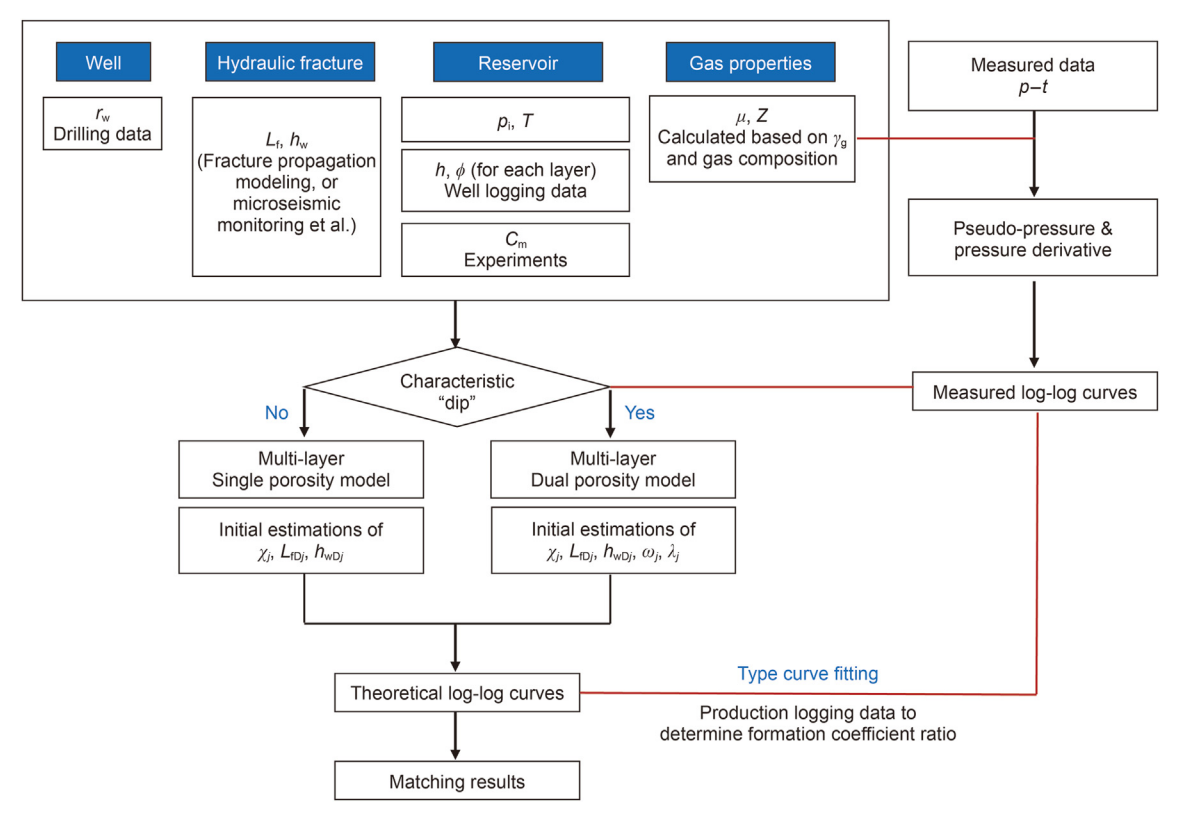


Fig. 23. The flow chart to obtain reservoir and fracture parameters with the proposed model.

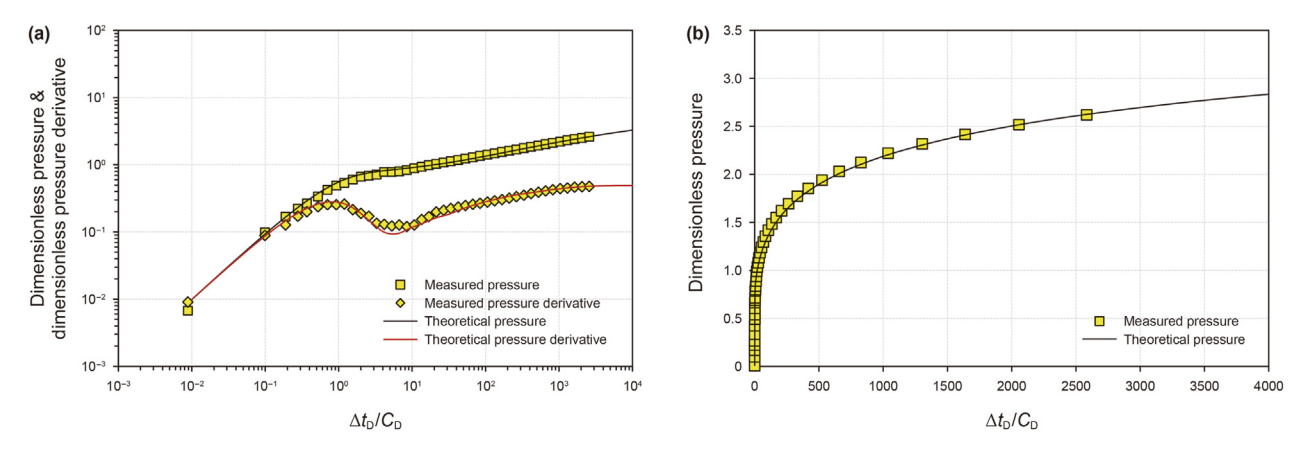


Fig. 24. (a) Pressure and pressure derivative matching of well A with the proposed model; (b) pressure history matching of well A.

obtain the layer parameters. The procedure and the matching results demonstrate that the proposed model is capable and feasible to determine the physical parameters for individual layers, and can provide technical support for performance analysis of multilayered tight gas reservoirs.

6.2. Case study 2

The proposed model is applied to analyze the transient pressure data collected from another gas well (well B) to further demonstrate its applicability. Well B is a commingle production gas well in the Sichuan Basin in China. It intersects two main production layers, and hydraulic fracturing is applied to each layer to obtain a commercial production rate. The reservoir temperature is 105 °C, and the specific gravity of the produced natural gas is 0.59. The wellbore radius is

0.0762 m. The pressure buildup test was conducted to obtain dynamic parameters of the reservoir and hydraulic fracture.

As shown in Fig. 25 (a), wellbore storage period, transitional flow period, linear flow period, and radial flow period with constant pressure derivative curve can be identified from the log-log plot of measured pressure and pressure derivative curves. In addition, a concave in the pressure derivative curve can also be observed during the late stage, which is commonly regarded as a reflection of dual porosity medium. Core analysis also indicates that there are natural fractures in reservoir rocks. Therefore, the proposed model for multi-layer dual porosity reservoirs was adopted to analyze the pressure buildup data.

The analysis of the transient well testing data of well B was conducted based on the workflow shown in Fig. 23. As illustrated in Fig. 25(a), the theoretical pressure and pressure derivatives

Table 5The interpretation results of well A.

| Parameter | Result | | |
|---|---------|---------|--|
| | Layer 1 | Layer 2 | |
| Half-length of hydraulic fracture, m | 32 | 28 | |
| Horizontal permeability of the formation, mD | 0.045 | 0.075 | |
| Permeability ratio k_{vi}/k_{hi} | 0.45 | 0.41 | |
| The ratio of the hydraulic fracture height to the formation thickness | 0.8 | 0.7 | |
| Skin factor | 0.65 | 0.73 | |
| Wellbore storage coefficient, m ³ /MPa | 0.62 | | |

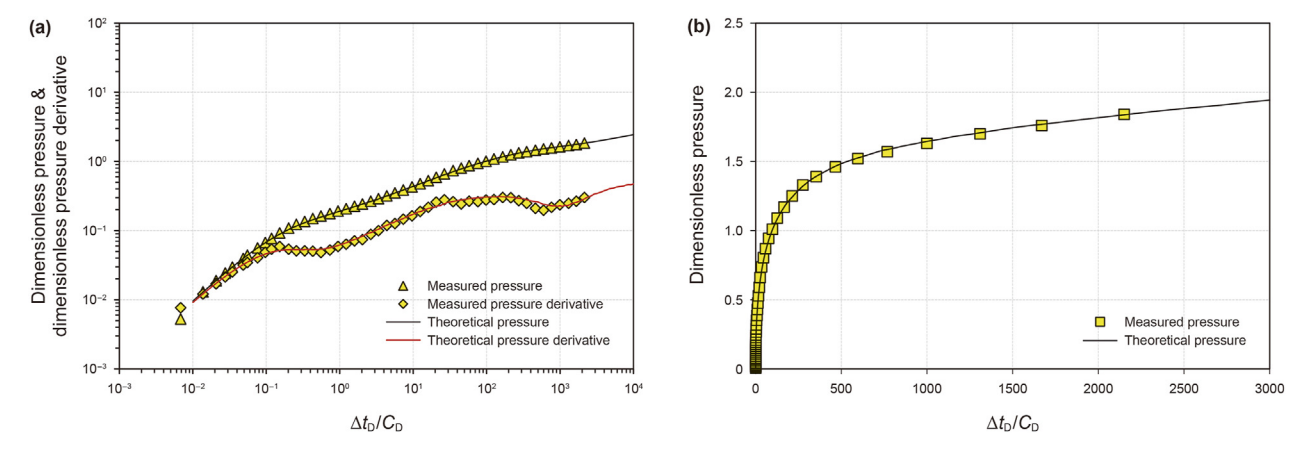


Fig. 25. (a) Pressure and pressure derivative matching of well B with the proposed model; (b) pressure history matching of well B.

Table 6The interpretation results of well B.

| Parameter | Result | | |
|---|-----------------------|-----------------------|--|
| | Layer 1 | Layer 2 | |
| Half-length of hydraulic fracture, m | 56 | 45 | |
| Horizontal permeability of the formation, mD | 0.086 | 0.041 | |
| Permeability ratio k_{vi}/k_{hi} | 0.48 | 0.42 | |
| The ratio of the hydraulic fracture height to the formation thickness | 0.76 | 0.71 | |
| Inter-porosity flowing coefficient of each layer | 1.21×10^{-6} | 0.87×10^{-6} | |
| Storativity ratio of each layer | 0.24 | 0.18 | |
| Skin factor | 0.11 | 0.07 | |
| Wellbore storage coefficient, m ³ /MPa | 0.78 | | |

calculated by the proposed model fit perfectly with the measured data, validating the reliability of the presented model. The corresponding interpretation results are shown in Table 6. Moreover, Fig. 25(b) also presents the pressure history matching results of well B, and a good agreement can also be observed, indicating that the interpretation results are reasonable and acceptable.

7. Conclusions

In this paper, we propose a semi-analytical model for fractured vertical wells with limited fracture height and unequal initial pressure in dual-porosity layered gas reservoirs. The proposed model is verified by comparison with a commercial software and by the matching with two field cases. Characteristic flowing regimes and the characteristics of production contribution from different layers are discussed, and a sensitivity analysis is conducted to identify prevailing influential factors. Based on the presented work, the following conclusions are obtained.

(1) Compared with the current models for fractured vertical wells in multi-layer gas reservoirs, the semi-analytical model

- proposed in this paper comprehensively takes into account the limited fracture height and multiple storage spaces in each layer, and is capable of determining the parameters of individual layers. The model can also be extended to investigate transient pressure dynamics of fractured wells in multilayer carbonate gas reservoirs or volcanic gas reservoirs, which are characterized by large thickness and co-presence of pores and natural fractures.
- (2) Seven flowing regimes can be identified based on the characteristics of transient pressure and pressure derivative curves, including the wellbore storage period, the transitional flowing period, the reservoir linear flow period, the vertical pseudo-radial flow period in the natural fracture system, the inter-porosity flow between natural fracture and matrix system (or the second linear flow period), the late-time pseudo-radial flow in the natural fracture and matrix systems, and the boundary-dominated flowing period.
- (3) Unequal initial formation pressures, half-length of hydraulic fracture, and fracture height have obvious influences on the transient pressure behavior of the commingled production well. Unequal initial formation pressure mainly affects the

transient pressure behavior during the transitional flowing period. Larger fracture half-length leads to a lower pressure derivative curve during the transitional flowing, the reservoir linear flow, and the vertical pseudo-radial flowing periods. As the penetration ratio of the hydraulic fracture increases, the position of the dimensionless pressure derivative curve during the reservoir linear flow period becomes lower. The influence of stress sensitivity becomes more obvious during late-time flowing periods. The parameters related to the dual porosity medium, i.e., the storativity ratio and the inter-porosity flowing coefficient, mainly affect the transient pressure behavior during the inter-porosity flowing period.

- (4) The gas production at the initial stage is mainly contributed by the high-pressure/high-permeability layer. When the pressure difference between different layers increases to a critical extent, gas backflow will occur during the early production. The difference between the production contributions of different layers gradually decreases as production time increases.
- (5) Two field case studies are conducted in the Sichuan Basin, and the proposed model show good agreement with field data, which indicates the accuracy and application prospect of the proposed model.

CRediT authorship contribution statement

Jing-Jing Guo: Writing — original draft, Software, Conceptualization. **Chao-Zhi Jiang:** Software, Investigation. **Hai-Tao Wang:** Validation, Methodology, Data curation. **Lie-Hui Zhang:** Writing — review & editing, Supervision, Funding acquisition.

Declaration of competing interest

The authors declare that they have no known competing financial interests or personal relationships that could have appeared to influence the work reported in this paper.

Acknowledgements

This work was financially supported by the National Natural Science Foundation of China (Grant Nos. 52174036, 52234003), the Sichuan Province Science and Technology Program (Grant No. 2024NSFSC0199), and the Joint Fund for Innovation and Development of Chongqing Natural Science Foundation (Grant No. 2023NSCQ-LZX0184).

Appendix A. Dimensional mathematical model of a pointsink in multi-layer dual porosity gas reservoirs

According to the physical model and corresponding assumptions presented in Section 2, the governing equations describing gas flowing in layer j in the multi-layer dual porosity reservoirs can be derived.

The permeability modulus is adopted to describe the stress sensitivity of fracture system, and the governing equation for the natural fracture system can be expressed as

$$\begin{split} &\frac{1}{r_{j}}\frac{\partial\left(r_{j}\frac{p_{fj}}{Z_{j}}\frac{k_{fhj0}e^{-\gamma_{j}\left(p_{fj0}-p_{fj}\right)}}{\mu_{j}}\frac{\partial p_{fj}}{\partial r_{j}}\right)}{\partial r_{j}}+\frac{\partial\left(\frac{p_{fj}}{Z_{j}}\frac{k_{fvj0}e^{-\gamma_{j}\left(p_{fj0}-p_{fj}\right)}}{\mu_{j}}\frac{\partial p_{fj}}{\partial z_{j}}\right)}{\partial z_{j}}\\ &=\phi_{fj}C_{fj}\frac{p_{fj}}{Z_{j}}\frac{\partial p_{fj}}{\partial t}-\frac{\alpha_{j}k_{mj}p_{rj}}{\mu_{j}Z_{j}}\left(p_{mj}-p_{fj}\right) \end{split} \tag{A1}$$

The governing equation for the matrix system is

$$\phi_{mj}C_{mj}\frac{p_{mj}}{Z_{j}}\frac{\partial p_{mj}}{\partial t} + \frac{\alpha_{j}k_{mj}p_{rj}}{\mu_{j}Z_{j}}\left(p_{mj} - p_{fj}\right) = 0 \tag{A2}$$

where the subscript j represents layer j ($j=1, 2, \dots, M$); r_j is the radial distance in layer j, $r_j = \sqrt{(x_j - x_{wj})^2 + (y_j - y_{wj})^2}$, m; x_j , y_j and z_i are the x-coordinate, y-coordinate and z-coordinate of an arbitrary point in layer j, respectively, m; x_{wi} , y_{wi} and z_{wi} are the xcoordinate, y-coordinate and z-coordinate of the point-sink in layer j, respectively, m; p_{fj} is the initial pressure of the natural fracture system in layer j, Pa; p_{mj} is the initial pressure of the matrix system in layer j, Pa; p_{rj} is the reference pressure, Pa; k_{fhj0} and k_{fvj0} are the horizontal and vertical permeabilities of the natural fracture system of layer i under the initial formation pressure, respectively, m²; γ_i is the permeability modulus, Pa⁻¹; k_{mj} is the permeability of the matrix system of layer j, m²; μ_j is the gas viscosity of layer j, Pa·s; Z_j is the gas deviation factor of layer j, dimensionless; C_{fi} and C_{mi} are the total compressibilities of the natural fracture system and the matrix system in layer j, respectively, Pa^{-1} ; ϕ_{fj} and ϕ_{mj} are the porosities of the natural fracture system and the matrix system in layer *j*, respectively, dimensionless; *t* is the production time, s.

The corresponding initial conditions of natural fracture system and matrix system are

$$p_{fj}(r_j, z_j, t)\Big|_{t=0} = p_{lj} \tag{A3}$$

$$p_{mj}(r_j, z_j, t)\Big|_{t=0} = p_{lj}$$
 (A4)

where p_{li} is the initial formation pressure of layer j, Pa.

The impermeable outer boundary conditions of layer j can be expressed as

$$\left. \frac{\partial p_{fj}(r_j, z_j, t)}{\partial z_j} \right|_{z_j = h_j} = 0 \ \ (impermeable lower boundary)$$
 (A7)

where r_{ej} is the radius of the outer boundary of layer j, m; h_j is the formation thickness of layer j, m.

Given that a continuous point-sink is located at point (x_{wj}, y_{wj}, z_{wj}) in layer j, and the production rate (under standard condition) of the point-sink is $\hat{q}_j(t)$. The corresponding inner boundary condition which takes stress sensitivity into account can be expressed as

$$\lim_{\epsilon_{j} \to 0} \int_{z_{wj} - \epsilon_{j}/2}^{z_{wj} + \epsilon_{j}/2} \left[\lim_{\sigma_{j} \to 0} \frac{2\pi k_{\text{fh}j0} e^{-\gamma_{j}(p_{\text{f}j0} - p_{\text{f}j})}}{\mu(p_{j})} \left(r_{j} \frac{\partial p_{\text{f}j}}{\partial r_{j}} \right)_{r_{j} = \sigma_{j}} \right] dz_{j}$$

$$= \widehat{q}_{j}(t) \frac{p_{\text{sc}} Z(p_{\text{f}j}) T}{p_{\text{f}j} T_{\text{sc}}}$$
(A8)

where ε_i is the infinitesimal variable in the vertical direction in layer j, m; σ_i is the infinitesimal variable in the radial direction in layer j, m; p_{sc} is the pressure under standard condition, Pa; T is the reservoir temperature, K; T_{SC} is the temperature under standard condition, K; $\hat{q}_i(t)$ is the production rate of the point-sink in layer j, m³/s.

To linearize the above partial differential equations, the concept of pseudo-pressures is introduced

$$\psi_{fj} = \int_{p_0}^{p_{fj}} \frac{2p_{fj}}{\mu(p_{fj})Z(p_{fj})} dp_{fj}$$
(A9a)

$$\psi_{mj} = \int_{p_0}^{p_{mj}} \frac{2p_{mj}}{\mu(p_{mj})Z(p_{mj})} dp_{mj}$$
 (A9b)

$$\psi_{lj} = \int_{p_0}^{p_{ij}} \frac{2p_j}{\mu(p_j)Z(p_j)} dp_j$$
 (A9c)

where ψ_{fj} is the pseudo-pressure of the natural fracture system in layer j, Pa/s; ψ_{mj} is the pseudo-pressure of the matrix system in layer j, Pa/s; ψ_{lj} is the pseudo-pressure of the initial formation pressure of layer j, Pa/s.

Using the definitions of pseudo-pressure, Eqs. (A1)–(A8) can be

$$\begin{split} k_{\text{fhj0}}h_{j} &\left\{ \frac{\partial^{2}\psi_{fj}}{\partial r_{j}^{2}} + \frac{1}{r_{j}} \frac{\partial\psi_{fj}}{\partial r_{j}} + \beta_{j} \left(\frac{\partial\psi_{fj}}{\partial r_{j}} \right)^{2} + \frac{k_{\text{fvj0}}}{k_{\text{fhj0}}} \left[\frac{\partial^{2}\psi_{fj}}{\partial z_{j}^{2}} + \beta_{j} \left(\frac{\partial\psi_{fj}}{\partial z_{j}} \right)^{2} \right] \right\} \\ &= \phi_{fj}\mu_{j}C_{fj}h_{j}e^{\beta_{j}(\psi_{fj0} - \psi_{fj})} \frac{\partial\psi_{fj}}{\partial t} - \alpha_{j}k_{mj}e^{\beta_{j}(\psi_{fj0} - \psi_{fj})}h_{j} \left(\psi_{mj} - \psi_{fj} \right) \end{split} \tag{A10}$$

$$\phi_{mj}h_{j}\mu_{j}C_{mj}\frac{\partial\psi_{mj}}{\partial t} + \alpha_{j}k_{mj}h_{j}\left(\psi_{mj} - \psi_{fj}\right) = 0 \tag{A11}$$

$$\psi_{fj}(r_j, z_j, t)\Big|_{t=0} = \psi_{Ij} \tag{A12}$$

$$|\psi_{mj}(r_j, z_j, t)|_{t=0} = \psi_{lj}$$
 (A13)

$$\frac{\partial \psi_{fj}(r_j, z_j, t)}{\partial z_j}\bigg|_{z_j = 0} = 0 \text{ (impermeable upper boundary)}$$
 (A15)

$$\lim_{\epsilon_{j}\to 0} \int_{z_{wj}-\epsilon_{j}/2}^{z_{wj}+\epsilon_{j}/2} \left[\lim_{\sigma_{j}\to 0} \frac{\pi k_{\text{fh}j0} T_{\text{sc}}}{p_{\text{sc}} T} \left(r_{j} e^{-\beta_{j} \left(\psi_{fj0} - \psi_{fj} \right)} \frac{\partial \psi_{fj}}{\partial r_{j}} \right)_{r_{j}=\sigma_{j}} \right] dz_{j} = \widehat{q}_{j}(t)$$
(A17)

where ψ_i is the pseudo-pressure of layer j, Pa/s; μ_{gi} is the gas viscosity evaluated under the initial formation pressure of layer *j*, Pa·s; C_{gj} is the gas compressibility evaluated under the initial formation pressure of layer j, Pa⁻¹; $\beta_i = \frac{\mu_j Z_j}{2n_{fi}} \gamma_j$, s/Pa.

Eqs. (A10)-(A17) are the dimensional mathematical model of a point-sink in multi-layer dual porosity gas reservoirs.

Appendix B. Dimensional mathematical model of a pointsink in multi-layer gas reservoirs with gas-water two-phase

The governing equations describing gas flowing in layer j in the multi-layer reservoirs can be derived as

$$\frac{1}{r_{j}} \frac{\partial}{\partial r_{j}} \left[\frac{k_{hj} k_{rgj}}{\mu_{gj}} \rho_{gj} r_{j} \left(\frac{\partial p_{j}}{\partial r_{j}} \right) \right] + \frac{\partial}{\partial z_{j}} \left[\frac{k_{vj} k_{rgj}}{\mu_{gj}} \rho_{gj} \left(\frac{\partial p_{j}}{\partial z_{j}} \right) \right] = \frac{\partial}{\partial t} \left(\rho_{gj} \phi_{j} S_{gj} \right)$$
(B1)

Similarly, the governing equations describing water flowing in layer j in the multi-layer reservoirs can be written as

$$\frac{1}{r_{j}}\frac{\partial}{\partial r_{j}}\left[\frac{k_{hj}k_{rwj}}{\mu_{wj}}\rho_{wj}r_{j}\left(\frac{\partial p_{j}}{\partial r_{j}}\right)\right] + \frac{\partial}{\partial z_{j}}\left[\frac{k_{vj}k_{rwj}}{\mu_{wj}}\rho_{wj}\left(\frac{\partial p_{j}}{\partial z_{j}}\right)\right] = \frac{\partial}{\partial t}\left(\rho_{wj}\phi_{j}S_{wj}\right) \tag{B2}$$

where S_{gj} and S_{wj} are the gas and water saturations in layer j, separately, dimensionless; K_{rgj} and K_{rwj} are the relative permeabilities of gas and water phase in layer *j*, separately, dimensionless.

By combining Eqs. (B1)–(B2), one can get the following equation to describe gas—water two-phase flow in layer j.

$$\frac{1}{r_{j}} \frac{\partial}{\partial r_{j}} \left[k_{hj} \left(\frac{k_{rgj}}{\mu_{gj}} \rho_{gj} + \frac{k_{rwj}}{\mu_{wj}} \rho_{wj} \right) r_{j} \left(\frac{\partial p_{j}}{\partial r_{j}} \right) \right]
+ \frac{\partial}{\partial z_{j}} \left[k_{vj} \left(\frac{k_{rgj}}{\mu_{gj}} \rho_{gj} + \frac{k_{rwj}}{\mu_{wj}} \rho_{wj} \right) \left(\frac{\partial p_{j}}{\partial z_{j}} \right) \right] = \frac{\partial}{\partial t} \left(\rho_{gj} \phi_{j} S_{gj} + \rho_{wj} \phi_{j} S_{wj} \right)$$
(B3)

Taylor expansion is adopted to simplify Eq. (B3), and we can obtain the following equation:

$$\begin{split} & \frac{1}{r_{j}} \frac{\partial}{\partial r_{j}} \left[k_{\text{h}j} \left(\frac{k_{\text{rg}j}}{\mu_{\text{g}j}} \rho_{\text{g}j} + \frac{k_{\text{rw}j}}{\mu_{\text{w}j}} \rho_{\text{w}j} \right) r_{j} \left(\frac{\partial p_{j}}{\partial r_{j}} \right) \right] + \frac{\partial}{\partial z_{j}} \left[k_{\text{v}j} \left(\frac{k_{\text{rg}j}}{\mu_{\text{g}j}} \rho_{\text{g}j} + \frac{k_{\text{rw}j}}{\mu_{\text{w}j}} \rho_{\text{w}j} \right) \right] \\ & \left(\frac{\partial p_{j}}{\partial z_{j}} \right) \right] = \phi_{j} C_{j} \frac{\partial p_{j}}{\partial t} \end{split}$$

(B4)

where $C_j = \rho_{gj0}C_{gj}S_{gj} + \rho_{wj0}C_{wj}S_{wj}$. The corresponding initial and boundary conditions are

$$p_j(r_j, z_j, t)\Big|_{t=0} = p_{lj}$$
 (B5)

$$\left. \frac{\partial p_j(r_j, z_j, t)}{\partial r_j} \right|_{r_i = r_{ej}} = 0 \text{ (impermeable lateral boundary)}$$
 (B6)

$$\frac{\partial p_j(r_j, z_j, t)}{\partial z_j}\bigg|_{z_i=0} = 0 \text{ (impermeable upper boundary)}$$
 (B7)

$$\frac{\partial p_j(r_j, z_j, t)}{\partial z_j} \bigg|_{z_j = h_j} = 0 \text{ (impermeable lower boundary)}$$
 (B8)

The inner boundary condition of the point-sink can thus be written as

$$\lim_{\epsilon_{j} \to 0} \int_{z_{wj} - \epsilon_{j}/2}^{z_{wj} + \epsilon_{j}/2} \left[\lim_{\sigma_{j} \to 0} 2\pi k_{hj} \left(\rho_{g} \frac{k_{rgj}}{\mu_{g}} + \rho_{w} \frac{k_{rwj}}{\mu_{w}} \right) \left(r_{j} \frac{\partial p_{j}}{\partial r_{j}} \right)_{r_{j} = \sigma_{j}} \right] dz_{j}$$

$$= \rho_{gsc} \hat{q}_{gscj} + \rho_{wsc} \hat{q}_{wscj}$$
(B9)

where \hat{q}_{gscj} is the gas production rate of the point-sink in layer j, m^3/s ; \hat{q}_{wscj} is the water production rate of the point-sink in layer j, m^3/s .

Similarly, the pseudo-pressure is adopted to linearize the governing equation. For gas—water two-phase flow, the pseudo-pressure is defined as follow:

$$m(p_{fj}) = \int_0^{p_j} \left(\frac{\rho_{gj} k_{rgj}}{\mu_{gj}} + \frac{\rho_{wj} k_{rwj}}{\mu_{wj}} \right) dp_j$$
 (B10)

Substituting Eq. (B10) into Eqs. (B4)–(B9), we can obtain the linearized diffusion equations, initial and boundary conditions of the multi-layer reservoirs:

$$\frac{\partial^{2} \psi_{j}}{\partial r_{j}^{2}} + \frac{1}{r_{j}} \left(\frac{\partial \psi_{j}}{\partial r_{j}} \right) + \frac{k_{vj}}{k_{hj}} \left(\frac{\partial^{2} \psi_{j}}{\partial z_{j}^{2}} \right) = \frac{\phi_{j} C_{j}}{k_{hj}} \frac{1}{\left(\frac{\rho_{gj} k_{rgj}}{\mu_{gj}} + \frac{\rho_{vj} k_{rvj}}{\mu_{vj}} \right)} \frac{\partial \psi_{j}}{\partial t}$$
(B12)

$$\psi_{i}(r_{j}, z_{j}, t)\big|_{t=0} = \psi_{lj}$$
 (B13)

$$\left. \frac{\partial \psi_j(r_j, z_j, t)}{\partial z_j} \right|_{z_i = 0} = 0 \quad \text{(impermeable upper boundary)} \tag{B15}$$

$$\frac{\partial \psi_j(r_j, z_j, t)}{\partial z_j}\bigg|_{z_j = b_j} = 0 \text{ (impermeable lower boundary)}$$
 (B16)

$$\lim_{\epsilon_{j} \to 0} \int_{z_{wj} - \epsilon_{j}/2}^{z_{wj} + \epsilon_{j}/2} \left[\lim_{\sigma_{j} \to 0} 2\pi k_{hj} \left(\rho_{g} \frac{k_{rgj}}{\mu_{g}} + \rho_{w} \frac{k_{rwj}}{\mu_{w}} \right) \left(r_{j} \frac{\partial p_{j}}{\partial r_{j}} \right)_{r_{j} = \sigma_{j}} \right] dz_{j}$$

$$= \rho_{gsc} \hat{q}_{gscj} + \rho_{wsc} \hat{q}_{wscj} \tag{B17}$$

Eqs. (B12)—(B17) are the dimensional mathematical model of a point-sink in multi-layer gas reservoirs with gas—water two-phase flow.

References

- Chai, X.L., Tian, L., Dong, P.J., Wang, C.Y., Peng, L., Wang, H.L., 2022. Study on recovery factor and interlayer interference mechanism of multilayer coproduction in tight gas reservoir with high heterogeneity and multi-pressure systems. J. Petrol. Sci. Eng. 210, 109699. http://dx.doi.org/10.1016/j.petrol.2021.109699.
- Cheng, M.H., Xue, W., Guo, Z., Hou, M.F., Wang, C.H., 2023. Development of large-scale tight gas sandstone reservoirs and recommendations for stable production—The example of the Sulige gas field in the Ordos Basin. Sustainability 15 (13), 9933. http://dx.doi.org/10.3390/su15139933.
- Ding, J.C., Yan, C.H., He, Y.M., Wang, C.C., 2019. Secondary formation damage of low-pressure layer during commingled production in multilayered tight gas reservoirs. Sci. Rep. 9, 17542. http://dx.doi.org/10.1038/s41598-019-53940-6.
- Fan, X., Huang, Z., Liu, Z., Zhang, J., Ji, Y., 2020. Complex stress state evaluation and its influence in the hydraulic fracture geometry of the Upper Triassic Xujiahe tight formation in the western Sichuan Basin of China. In: SPE/AAPG/SEG Unconventional Resources Technology Conference. http://dx.doi.org/10.15530/urtec-2020-2620.
- Gao, C., Jones, J.R., Raghavan, R., Lee, W.J., 1994. Responses of commingled systems with mixed inner and outer boundary conditions using derivatives. SPE Form. Eval. 9 (4), 264–271. http://dx.doi.org/10.2118/22681-PA.
- Gomes, E., Ambastha, A.K., 1993. An analytical pressure-transient model for multilayered, composite reservoirs with pseudosteady-state formation crossflow. In: SPE Western Regional Meeting. http://dx.doi.org/10.2118/26049-MS.
- Gringarten, A.C., Ramey Jr., H.J., Raghavan, R., 1974. Unsteady-state pressure distributions created by a well with a single infinite-conductivity vertical fracture. SPE J. 14 (4), 347–360. http://dx.doi.org/10.2118/4051-PA.
- Guo, J.C., Lu, Q.L., Liu, Z., Zeng, F.H., Guo, T.L., Liu, Y., Liu, L., Qiu, L., 2023. Concept and key technology of "multi-scale high-density" fracturing technology: A case study of tight sandstone gas reservoirs in the western Sichuan Basin. Nat. Gas. Ind. B 10 (3), 283–292. http://dx.doi.org/10.1016/j.ngib.2023.05.005.
- Jia, C.Z., 2017. Breakthrough and significance of unconventional oil and gas to classical petroleum geology theory. Petrol. Explor. Dev. 44 (1), 1–10. http:// dx.doi.org/10.1016/S1876-3804(17)30002-2.
- Jiang, F.J., Jia, C.Z., Pang, X.Q., Jiang, L., Zhang, C.L., Ma, X.Z., Qi, Z.G., Chen, J.Q., Pang, H., Hu, T., Chen, D.X., 2023. Upper Paleozoic total petroleum system and geological model of natural gas enrichment in Ordos Basin, NW China. Petrol. Explor. Dev. 50 (2), 250–261. http://dx.doi.org/10.1016/S1876-3804(23)60387-8.
- Jiang, L., Zhao, W., Bo, D.M., Hong, F., Gong, Y.J., Hao, J.Q., 2023. Tight sandstone gas accumulation mechanisms and sweet spot prediction, Triassic Xujiahe Formation, Sichuan Basin, China. Pet. Sci. 20 (6), 3301–3310. http://dx.doi.org/10.1016/ j.petsci.2023.07.008.
- Lefkovits, H.C., Hazebroek, P., Allen, E.E., Matthews, C.S., 1961. A study of the behavior of bounded reservoir composed of stratified layers. SPE J. 1 (1), 43–58. http://dx.doi.org/10.2118/1329-G.
- Li, M., Su, Y.L., Wang, W.D., Li, Y.J., Dong, M.Z., 2022. Impact of cross-flow on well production in shale reservoir considering vertical variation of reservoir and fracture properties: model and field application. J. Petrol. Sci. Eng. 208, 109739. http://dx.doi.org/10.1016/j.petrol.2021.109739.
- Liang, W., Wang, J.G., Leung, C.F., Goh, S., Li, P.B., 2023. Impact of crossflow and twophase flow on gas production from stacked deposits. Energy & Fuels 37 (13), 8935–8948. http://dx.doi.org/10.1021/acs.energyfuels.3c00654.
- Liu, G.F., Meng, Z., Luo, D.Y., Wang, J.N., Gu, D.H., Yang, D.Y., 2020. Experimental evaluation of interlayer interference during commingled production in a tight sandstone gas reservoir with multi-pressure systems. Fuel 262, 116557. http:// dx.doi.org/10.1016/j.fuel.2019.116557.
- Liu, Y.W., Zhu, W.Y., Kong, D.B., Pan, B., Yue, M., 2022. Analytical model of hydraulic fracturing horizontal well gas production capacity of a water-bearing tight sandstone reservoir considering planar heterogeneity. Phys. Fluids 34 (12), 126603. http://dx.doi.org/10.1063/5.0128769.
- Lu, J., Zhou, B.T., Rahman, M.M., He, X.M., 2019. New solution to the pressure transient equation in a two-layer reservoir with crossflow. J. Comput. Appl. Math. 362, 680–693. http://dx.doi.org/10.1016/j.cam.2018.05.065.
- Manrique, J.F., Poe, B.D., 2009. A unique methodology for evaluation of multi-fractured wells in stacked-pay reservoirs using commingled production and rate transient analysis. In: SPE Annual Technical Conference and Exhibition. http://dx.doi.org/10.2118/110576-MS.
- Meng, D.W., Jia, A.L., He, D.B., 2016. Water and gas distribution and its controlling factors of large scale tight sand gas fields: A case study of western Sulige gas field, Ordos Basin, NW China. Petrol. Explor. Dev. 43 (4), 663–671. http:// dx.doi.org/10.1016/S1876-3804(16)30077-5.
- Osman, M.E., 1993. Pressure analysis of a fractured well in multilayered reservoirs.

 J. Petrol. Sci. Eng. 9 (1), 49–66. http://dx.doi.org/10.1016/0920-4105(93)90028-D.
- Ozkan, E., Raghavan, R., 1991. New solutions for well-test-analysis problems: Part 1-analytical considerations. SPE Form. Eval. 6 (3), 359–368. http://dx.doi.org/

10.2118/18615-PA.

- Rahman, N.M.A., Matter, L., 2007. New analytical solution to pressure transient problems in commingled, layered zones with unequal initial pressures subject to step changes in production rates. J. Petrol. Sci. Eng. 56 (4), 283–295. http://dx.doi.org/10.1016/j.petrol.2006.10.002.
- Santiago, V., Ribeiro, A., Hurter, S., 2021. Modeling the contribution of individual coal seams on commingled gas production. SPE Prod. Oper. 36 (1), 245–261. http://dx.doi.org/10.2118/198241-PA.
- Scott, M.P., Stephens, R.H., McGowen, J.M., Thom, W.W., Woodroof, R.A., 2013. Investigating hydraulic fracturing in tight gas sand and shale gas reservoirs in the Cooper Basin. In: SPE Unconventional Resources Conference and Exhibition— Asia Pacific, http://dx.doi.org/10.2118/167073-MS.
- Shi, W.Y., 2021. Well Test Model of Typical Gas Reservoir in Western Sichuan Depression and its Application. Doctoral Dissertation. China University of Petroleum. Beijing.
- Shi, W.Y., Yao, Y.D., Cheng, S.Q., Shi, Z.L., Wang, Y., Zhang, J., Zhang, C.W., Gao, M., 2020a. Pressure transient behavior and flow regimes characteristics of vertical commingled well with vertical combined boundary: A field case in XC gas field of northwest Sichuan Basin, China. J. Petrol. Sci. Eng. 194, 107481. http://dx.doi.org/10.1016/j.petrol.2020.107481.
- Shi, W.Y., Yao, Y.D., Cheng, S.Q., Shi, Z.L., 2020b. Pressure transient analysis of acid fracturing stimulated well in multilayered fractured carbonate reservoirs: A field case in Western Sichuan Basin, China. J. Petrol. Sci. Eng. 184, 106462. http://dx.doi.org/10.1016/j.petrol.2019.106462.
- Stehfest, H., 1970. Algorithm 368: Numerical inversion of Laplace transforms. Communications of the Association for Computing Machinery 13 (1), 47–49. http://dx.doi.org/10.1145/361953.361969.
- Sun, H.L., Ning, Z.F., Yang, X.T., Lu, Y.H., Jin, Y., Chen, K.P., 2017. An analytical solution for pseudosteady-state flow in a hydraulically fractured stratified reservoir with interlayer crossflows. SPE J. 22 (4), 1103–1111. http://dx.doi.org/10.2118/185163-PA
- Tao, X.J., Okere, C.J., Su, G.D., Zheng, L.H., 2022. Experimental and theoretical evaluation of interlayer interference in multi-layer commingled gas production of tight gas reservoirs. J. Petrol. Sci. Eng. 208, 109731. http://dx.doi.org/10.1016/ i.petrol.2021.109731.
- van Everdingen, A.F., Hurst, W., 1949. The application of the Laplace transformation to flow problems in reservoirs. J. Petrol. Technol. 1 (12), 305–324. http://dx.doi.org/10.2118/949305-G
- Wang, F.Y., Liu, Z.C., Yue, H., 2023. Prediction of gas-water relative permeability in

- tight rock from movable fluid distribution with nuclear magnetic resonance. Phys. Fluids 35 (3), 033609. http://dx.doi.org/10.1063/5.0141543.
- Wang, H.T., 2014. Performance of multiple fractured horizontal wells in shale gas reservoirs with consideration of multiple mechanisms. J. Hydrol. 510, 199–312. http://dx.doi.org/10.1016/j.jhydrol.2013.12.019.
- Wang, L., He, Y.M., Wang, Q., Liu, M.M., Jin, X., 2021. Improving tight gas recovery from multi-pressure system during commingled production: An experimental investigation. Nat. Resour. Res. 30, 3673–3694. http://dx.doi.org/10.1007/ s11053-021-09869-7.
- Wang, Y.J., Kang, Y.L., You, L.J., Chen, M.J., Cheng, Y.Y., Tu, Y.Q., Tian, J., 2024. Effect of pore-throat heterogeneity on gas—water flow in tight gas reservoirs: From micro- to centimeter scale. Energy & Fuels 38 (6), 5075—5087. http://dx.doi.org/10.1021/acs.energyfuels.3c04230.
- Wei, C., Li, H.T., Luo, H.W., Li, Y., Cheng, S.Q., 2024. Generalized analytical solutions of vertically fractured wells in commingled reservoirs: Field case study. SPE J. 29 (3), 1419–1433. http://dx.doi.org/10.2118/218391-PA.
- Yuan, R., Jin, L., Zhu, C.L., Zhou, M., Vitthal, S., 2013. Vertical or horizontal? Hydraulic fracture geometry as a make or break to a tight gas field in the western Sichuan basin. In: International Petroleum Technology Conference. http://dx.doi.org/10.2523/IPTC-16757-MS.
- Zhang, M., Nguyen, K., Wang, Z.Q., Ayala, L.F., 2023. Flowback and early-time production modeling of unconventional gas wells using an improved semi-analytical method. Pet. Sci. 20 (6), 3441–3449. http://dx.doi.org/10.1016/i.petsci.2023.06.003.
- Zhang, T., Zhang, L., Wang, Y.K., Qiao, X.Y., Feng, D., Zhao, W., Li, X.F., 2020. An integrated well-pattern optimization strategy to unlock continental tight gas reservoir in China. Energy 209, 118449. http://dx.doi.org/10.1016/j.energy.2020.118449.
- Zhang, T., Wang, B.R., Zhao, Y.L., Zhang, L.H., Qiao, X.Y., Zhang, L., Guo, J.J., Thanh, H.V., 2024. Inter-layer interference for multi-layered tight gas reservoir in the absence and presence of movable water. Pet. Sci. 21 (3), 1751–1764. http://dx.doi.org/10.1016/j.petsci.2024.01.009.
- Zhang, Y.H., Yang, D.Y., 2021. Modeling transient pressure behaviour of a multi-fractured horizontal well in a reservoir with an arbitrary boundary and different fracture networks by considering stress-sensitive effect. J. Hydrol. 600, 126552. http://dx.doi.org/10.1016/j.jhydrol.2021.126552.
- Zou, C.N., Zhu, R.K., Liu, K.Y., Su, L., Bai, X., Zhang, X.X., Yuan, X.J., Wang, J.H., 2012. Tight gas sandstone reservoirs in China: Characteristics and recognition criteria. J. Petrol. Sci. Eng. 88–89, 82–91. http://dx.doi.org/10.1016/j.petrol.2012.02.001.